Carbon Neutrality

REVIEW Open Access

Fundamentals and economic analysis of hydrate-based carbon dioxide sequestration

Faping Liu[1], Yanhong Wang[1], Xuemei Lang[1,2], Gang Li[1] and Shuanshi Fan[1,2*]

Abstract

Fundamental research and economic analysis of hydrate-based carbon dioxide (CO_2) sequestration play a key role in developing the industrialization of oceanic CO_2 sequestration. Therefore, this review deals with recent progress in hydrate-based CO_2 sequestration from the thermodynamics and kinetics as well as their energy consumption and cost. The first section provides an overview of the thermodynamics of CO_2 hydrate formation in both pure water and sea water, establishing a relationship between the enthalpy change of the hydrate formation reaction and the hydrate structure. Subsequently, a comparison of the kinetics of CO_2 hydrate formation in pure water and sea water is presented, with further insight into the formation kinetics obtained through hydrate nucleation and growth models. The process of liquid CO_2 forming hydrates is summarized, serving as a critical part of the fundamental research for oceanic CO_2 sequestration. Finally, energy consumption and cost of CO_2 capture methods are compared, and the whole sequestration process cost of CO_2 capture-storage-transport-injection is comprehensively analyzed. The new understanding of this review is conducive to further commercial and industrial development of hydrate-based CO_2 sequestration.

Keywords Hydrate-based CO_2 sequestration, CO_2 hydrates, Thermodynamics, Kinetics, Model, Economic analysis

1 Introduction

With the advancement of human society and industry, fossil fuel use has led to significant carbon dioxide (CO_2) emissions, reaching approximately 143 million metric tons of carbon emissions [1]. CO_2 concentration in the atmosphere has been increasing constantly, rising to 413.8 ppm with 2.4 ppm/year increase by 2021 [2, 3]. As a major greenhouse gas, the substantial release of CO_2 has triggered a range of climate and environmental challenges, such as global warming [4] and sea level rise [5]. Since pre-industrial times, the global temperature has already increased by 1.0 °C, which has prompted the Paris Agreement's goal to limit global warming to 1.5 °C above pre-industrial levels [6]. Thus, CO_2 capture and sequestration to mitigate emissions is increasingly urgent. Compared to conventional CO_2 sequestration approaches, hydrate technology offers a novel approach, which can stabilize it as solid CO_2 hydrate in the ocean. In regions deeper than 300 m, CO_2 can be stably isolated through seabed disposal using hydrate technology [7–11]. Theoretical assessments indicated that hydrate-based oceanic CO_2 sequestration could reach 100 trillion tons, vastly exceeding terrestrial storage potential. A comprehensive understanding of the thermodynamics and kinetics of CO_2 hydrate formation, coupled with an economic analysis, is essential for advancing the industrialization of hydrate-based CO_2 sequestration.

The phase equilibrium temperature and pressure for CO_2 hydrate formation are influenced by the presence of salt ions in seawater, as well as the state of CO_2 and water. The presence of salt ions shifted the phase equilibrium line to the left, necessitating higher pressure for hydrate formation at the same temperature [12]. Once CO_2 was

*Correspondence:
Shuanshi Fan
ssfan@scut.edu.cn
[1] School of Chemistry and Chemical Engineering, South China University of Technology, Guangzhou 510640, China
[2] Key Laboratory of Fuel Cell Technology of Guangdong Province, Guangzhou 510640, China

liquefied, the phase equilibrium pressure for hydrate formation increased linearly [13]. Furthermore, the presence of salt ions reduced the enthalpy change of the CO_2 hydrate formation reaction by affecting the solubility of CO_2 [12]. The Clausius–Clapeyron equation provided a means to calculate the enthalpy change associated with hydrate formation [14]. In the presence of additives, the hydrate might transition to the sII-type structure, significantly increasing the enthalpy change of the hydrate formation reaction [15]. The enthalpy change is closely related to the type of hydrate [14, 15], so it is necessary to understand the thermodynamics of CO_2 hydrate formation.

Furthermore, the understanding of CO_2 hydrate formation is critical in developing hydrate-based CO_2 sequestration, as the rate and stability of hydrate formation directly impact the feasibility of sustained injection, as well as the sealing capacity and long-term stability of hydrate reservoirs. Yamasaki et al. [16–19] applied a seabed burial method to manage CO_2 emissions from Jiang's power plants, and their experimental and simulation results demonstrated that CO_2 could be fully converted to hydrate on the seabed, with hydrate particles capable of long-distance transport in the ocean [16]. A large-scale field test of CO_2 hydrate sequestration was also conducted in Monterey Bay [20, 21] and off the central coast of California [22]. In these tests, 40.0% of CO_2 gas was converted to hydrates at depths of 1000–1300 m under temperatures of 3.3–3.9 °C. The salt ions present in seawater significantly decreased both the gas storage capacity and the growth rate of CO_2 hydrates [23, 24]. Consequently, several techniques to enhance hydrate formation have been developed. Additionally, economic analysis is the critical in developing the industrial development of oceanic CO_2 sequestration. Through economic comparisons, more cost-effective sequestration methods can be identified, encompassing optimal strategies for CO_2 capture, storage, transportation, and injection into the seafloor.

Currently, most research has focused on the potential of hydrate-based oceanic CO_2 sequestration and the fundamental studies of CO_2 hydrate formation [25–34]. These fundamental studies are primarily oriented toward applications such as CO_2 capture and separation, as well as CH_4-CO_2 replacement, and are predominantly focused on gaseous-phase CO_2 [27–34]. However, during the process of hydrate-based oceanic CO_2 sequestration, salt ions in seawater significantly affect hydrate formation, and in marine environments, when water depth exceeds 450 m, CO_2 undergoes a phase transition from gas to liquid. Therefore, it is critical to investigate the process of hydrate formation from liquid CO_2. There is a lack of comparative analysis between the thermodynamics and kinetics in seawater and pure water, as well as an absence of economic analysis regarding the industrialization of this technology. To further develop hydrate-based CO_2 sequestration and avoid the problem caused by the process of CO_2 injection, fundamentals and economic analysis in CO_2 capture and sequestration have become a hot research field and have attracted more attention. This review will focus on three topics: (1) Thermodynamics of CO_2 hydrate formation in seawater and pure water; (2) Kinetics of CO_2 hydrate formation involving liquid CO_2; (3) Energy consumption and cost of hydrate-based CO_2 sequestration.

2 Thermodynamics of CO_2 hydrate formation

2.1 Thermodynamics of CO_2 hydrate formation in pure water and sea water

CO_2 hydrates are non-stoichiometric, ice-like crystals formed by CO_2 and water molecules under high-pressure, low-temperature conditions, with CO_2 molecules encapsulated in cage-like cavities formed by hydrogen bonds between water molecules. CO_2 hydrates form cubic sI crystal structures, and their structural unit consists of six tetrakaidecahedrons ($5^{12}6^2$: 12 pentagonal and 2 hexagonal faces) and two dodecahedrons (5^{12}: 12 pentagonal faces) [35]. CO_2 preferentially occupies the large cages in hydrate cages [36, 37]. The hydrate formation process is significantly influenced by the phase states of CO_2 and water, which can lead to variations in the enthalpy change associated with hydrate formation. The process of CO_2 hydrate formation can be regarded as a pseudo-chemical reaction as follows:

$$CO_2(g) + nH_2O(s) \rightarrow CO_2 \bullet nH_2O(s) \quad (1)$$

$$CO_2\,(g) + nH_2O(l) \rightarrow CO_2 \bullet nH_2O(s) \quad (2)$$

$$CO_2(l) + nH_2O(l) \rightarrow CO_2 \bullet nH_2O(s) \quad (3)$$

where $CO_2(g)$ represents gas CO_2, $nH_2O(s)$ represents solid ice, $CO_2 \bullet nH_2O(s)$ represents solid hydrate, $CO_2(l)$ represents liquid CO_2, $nH_2O(l)$ represents liquid water.

When the temperature falls below the freezing point, gaseous CO_2 and solid ice can combine to form solid hydrates, with the enthalpy changes of the hydration reaction ranging from 23.0 to 24.0 kJ/mol, as illustrated in the Fig. 1. At the freezing point, a unique point of four-phase equilibrium, Q1(V-H-I-Lw), emerges. The region to the left of the blue phase equilibrium curve represents the stability zone of CO_2 hydrates, while the region to the right indicates their instability. As indicated by Eqs. 1 and 2, the presence of liquid water necessitates the transition to ice, significantly increasing the enthalpy change of hydrate formation. The enthalpy change associated with

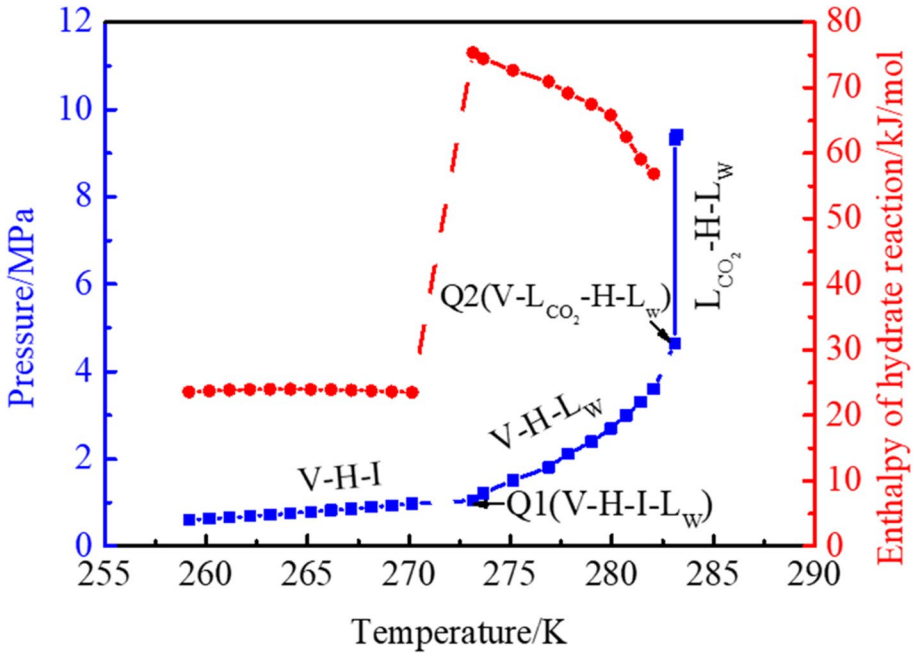

Fig. 1 Phase equilibrium pressure and temperature of CO_2 hydrates and corresponding enthalpy changes of hydrate reaction (V: Gas CO_2; H: Hydrate; I: Ice; Lw: Liquid water; L_{CO2}: Liquid CO_2) [13, 38, 40]

each mole of liquid water converting into ice was 6.0 kJ/mol [38]. Therefore, the enthalpy change associated with the transformation of ice into hydrates was lower than that associated with the transformation of liquid water into hydrates. When temperature decreased below 225 K, the activation energy for permeation of CO_2 molecules fell to 19.0 kJ/mol, which showed that ice was conductive to CO_2 hydrate formation [39]. Once ice fully was transitioned into liquid water, the equilibrium pressure progressively increased with temperature, while the enthalpy changes of the hydration reaction exhibit a declining trend. Within the temperature range of 273.2–282.1 K, the enthalpy change varied between 75.4 and 56.9 kJ/mol [40]. Another four-phase equilibrium point, Q2(V-L_{CO2}-H-Lw), involves gas CO_2, liquid CO_2, solid hydrate, and liquid water, which is attributed to CO_2 being in a gas–liquid equilibrium state. Once CO_2 is fully liquefied, the equilibrium pressure of the hydrate shows a linear increase. Notably, as the temperature increased from 283.1 K to 283.2 K, the pressure experienced a sharp rise from 4.65 MPa to 9.43 MPa, which was attributed to CO_2 liquefaction causing a rapid increase in phase equilibrium pressure [13]. For gaseous CO_2, an increase in pressure raises the phase equilibrium temperature, thereby enhancing the temperature driving force for hydrate formation. However, once CO_2 has liquefied, further pressure increases do not affect the phase equilibrium temperature, and thus do not enhance the temperature driving force. In contrast to gaseous CO_2, liquid CO_2 cannot promote hydrate formation by increasing pressure. Furthermore, compared to liquid water, the direct transformation of ice into a hydrate releases significantly less heat, thereby reducing the energy consumption of hydrate technology [41].

In addition to the phase states of liquid CO_2 and water, the presence of salt ions in seawater also influences the phase equilibrium of CO_2 hydrates and alters the enthalpy change associated with hydrate formation. The presence of salt ions not only shifts the phase equilibrium of CO_2 hydrate to the left but also reduces the enthalpy change of the hydrate formation reaction by lowering the enthalpy of CO_2 dissolution, as shown in Fig. 2. At the same phase equilibrium temperature, the phase equilibrium pressure of CO_2 hydrates in seawater was 0.4–0.5 MPa higher than that in pure water [12]. At 277.5 K, the hydrate phase equilibrium pressure of pure water was 2.13 MPa, whereas that of seawater was 2.53 MPa. As the temperature increased, the difference in the enthalpy changes of the hydrate formation reaction between pure water and seawater became more pronounced. At 277.5 K, the enthalpy change of hydrate formation in pure water was 56.9 kJ/mol, which was higher than 53.2 kJ/mol in seawater. At 278.7 K, the enthalpy change in pure water was 56.1 kJ/mol, compared to 49.7 kJ/mol in seawater. Therefore, it can be observed that in seawater, the heat released during the hydrate formation process is lower, which leads to a reduction in the energy consumption required for heat removal. However, salt ions hinder

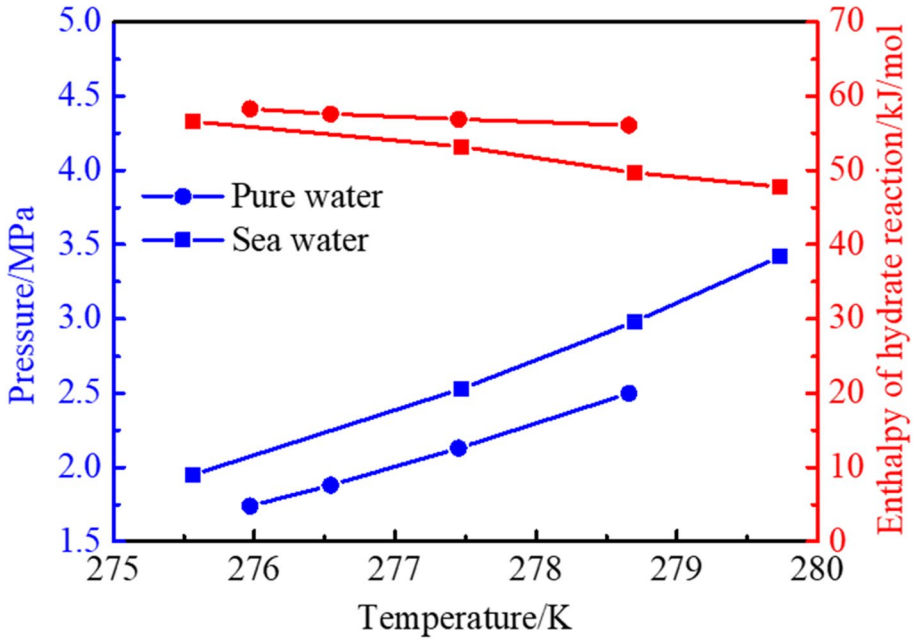

Fig. 2 Phase equilibrium pressure and temperature of CO_2 hydrates and corresponding enthalpy changes of hydrate reaction in pure water or seawater [12]

the formation of CO_2 hydrates, meaning that, at the same experimental temperature, higher pressures are required in seawater compared to pure water to form hydrates.

The enthalpy changes of the CO_2 hydrate formation reaction can be derived from the hydrate dissociation enthalpy, which can be measured using calorimetry [42–45] or the Clausius–Clapeyron equation [38, 46, 47]. Calorimetry is a direct measurement technique, typically performed with a calorimeter or differential scanning calorimeter (DSC). In contrast, the Clausius–Clapeyron equation provides an indirect method for calculating the enthalpy change. This equation describes the differential pressure change (dP) that accompanies a differential temperature change (dT) in a phase equilibrium system, and is calculated using Eq. 4 [38].

$$\frac{dP}{dT} = \frac{\Delta H}{T\Delta V} = \frac{\Delta H_{dis}}{T\Delta V} \tag{4}$$

where P represents the phase equilibrium pressure, T represents the corresponding temperature, ΔH_{dis} represents the hydrate dissociation enthalpy, ΔV represents the volume change for reaction. When 1 mol of hydrate decomposes, n moles of water are produced, and $nx(CO_2)$ dissolves in the water. The volume change for reaction ΔV is calculated by Eq. 5 [38].

$$\Delta V/\left(\mathrm{m^3/mol}\right) = 1 - nx(CO_2)l - x(CO_2)V(CO_2) + n\left(1.8\times10^{-5} + 2.04\times10^{-5}x(CO_2)\right) - 1.389\times10^{-4} \tag{5}$$

where n represents the moles of water, $x(CO_2)$ represents the molar fraction of CO_2 dissolves in the water, $V(CO_2)$ represents the volume of CO_2.

A comparison using the Clausius–Clapeyron equation also revealed that the presence of salt ions in seawater decreased the solubility of CO_2 in water, thereby influencing the phase volume change and leading to a lower enthalpy of hydrate formation reaction in seawater compared to pure water.

2.2 Thermodynamics of CO_2 hydrate formation with additives

To enable the formation of CO_2 hydrates under milder temperature and pressure conditions, thermodynamic additives present a viable solution. The various structures of CO_2 hydrates in the presence of different additives are depicted in Fig. 3. CO_2 can also form face-centered cubic sII hydrate with compounds including cyclopentane (CP) [35], cyclopentanone (CP-one) [48], cyclopentanol (CP-ol) [48], 1,4-dioxane (DXN) [49], tetrahydrofuran (THF) [49], and methylcyclopentane (MCP) [50]. The sII hydrate structural unit consists of eight hexakaidecahedrons ($5^{12}6^4$: 12 pentagonal and 4 hexagonal faces) and sixteen dodecahedrons (5^{12}: 12 pentagonal faces). The cages ($5^{12}6^4$) are occupied by additives, and the cages

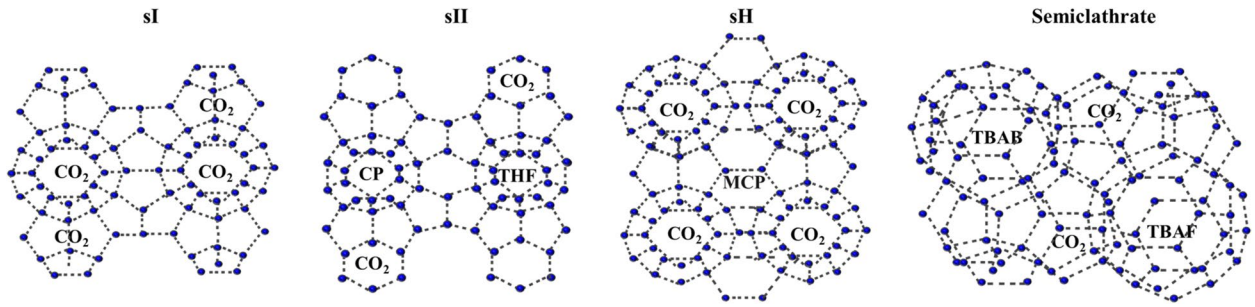

Fig. 3 Structures of CO_2 hydrates: sI hydrate, sII hydrate, sH hydrate and semi-clathrate hydrate

(5^{12}) are occupied by CO_2 molecules. CO_2 can also form hexagonal sH hydrate with 3,3-dimethyl-1-butanol (DMB) [51, 52] or neopentane (NH) [53]. The structural unit of sH hydrate includes one icosahedron ($5^{12}6^8$: 12 pentagonal and 8 hexagonal faces), three dodecahedrons (5^{12}: 12 pentagonal faces), and two irregular dodecahedrons ($4^35^{12}6^3$: 3 quadrilateral, 12 pentagonal, and 3 hexagonal faces). The cages ($5^{12}6^8$) are occupied by additives, and the cages (5^{12} and $4^35^{12}6^3$) are occupied by CO_2 molecules. CO_2 also forms tetragonal and orthorhombic semi-clathrate hydrates with additives such as tetrabutylammonium bromide (TBAB), tetrabutylammonium chloride (TBAC), and tetrabutylammonium fluoride (TBAF) [54–58]. The orthorhombic semi-cage hydrate unit consists of six dodecahedrons (5^{12}), four tetrakaidecahedrons ($5^{12}6^2$), and four pentakaidecahedrons ($5^{12}6^3$). The cages ($5^{12}6^2$ and $5^{12}6^3$) are occupied by tetrabutylammonium ions (TBA^+), and the cages (5^{12}) are occupied by CO_2 molecules. The presence of salts exhibits negligible impact on the overall crystal structures of structure I (sI), structure II (sII), and semi-clathrate hydrates [59, 60]. In aqueous NaCl solutions ranging from 3.6 to 10.0 wt%, the Raman spectral peaks of CO_2 hydrates closely resembled those observed in pure water systems, suggesting that the sI hydrate structure was preserved despite the presence of salt ions [59]. When tetrahydrofuran (THF) was added, THF molecules occupied the large cages while CO_2 occupied the small cages, leading to the formation of sII hydrates. In addition, the incorporation of LiCl did not alter the melting temperature of CO_2 hydrates, provided that sufficient free water was available to fully hydrate the LiCl [60].

After the addition of additives, the change in CO_2 hydrate structures can influence the hydrate formation temperature and pressure, and corresponding enthalpy change, as shown in Fig. 4. Three ammonium-based ionic liquids (tetramethylammonium chloride (TMACl), tetraethylammonium hydroxide (TEAOH), and tetrapropylammonium hydroxide (TPrAOH)) all inhibited CO_2 hydrate formation, shifting the phase equilibrium line to the left [61]. The inhibitory effect increased with the concentration of the ionic liquids. Specifically, TEAOH, TMACl and TPrAOH decreased the hydrate formation temperature by 1.7 K, 1.6 K, and 1.2 K. However, the average enthalpy changes for hydrate formation reaction with these ionic liquids ranged from 63.0 to 64.0 kJ/mol, which were very close to that of the pure water in the absence of ionic liquids, indicating that these ionic liquids did not participate in the formation of the CO_2 hydrate structures. Therefore, based on the enthalpy changes, it could be inferred that only the sI CO_2 hydrate structure was formed. In contrast, sII-type hydrates in the presence of THF and CP were formed, and these not only shifted the phase equilibrium line significantly to the right but also increased the average enthalpy change of hydrate formation to between 120.0 and 160.0 kJ/mol [14]. For 6.0 mol% CP, the phase equilibrium temperatures were 287.39–292.10 K at pressures ranging from 1.08 to 2.92 MPa. In the aqueous solution with 2.6 mol% THF, the phase equilibrium temperatures ranged from 285.18 to 290.30 K at pressures between 1.01 and 3.06 MPa. When the hydrate structure transitioned from sI hydrate to sII hydrate, the enthalpy changes of hydrate formation approximately doubled. After the addition of TBAC and TBAB, the phase equilibrium pressure of CO_2 hydrate formation decreased significantly, and the average enthalpy change of hydrate formation exceeded 200.0 kJ/mol, nearly three times higher than in the system without additives [14, 15, 62]. In the aqueous solution of 3.3 mol% TBAC, the phase equilibrium temperatures ranged from 292.2 to 293.0 K at pressures between 2.05 and 3.53 MPa, with an average enthalpy change of 336.3 kJ/mol [62]. In the aqueous solution with 1.7 mol% TBAB, the phase equilibrium temperatures ranged from 286.84 to 290.33 K at pressures between 0.90 and 3.01 MPa, with a corresponding enthalpy change of 205.8 kJ/mol [14]. After the addition of thermodynamic promoters, hydrate formation releases more heat, necessitating continuous heat removal to ensure the ongoing growth of the hydrates. Compared to the semi-clathrate and sII

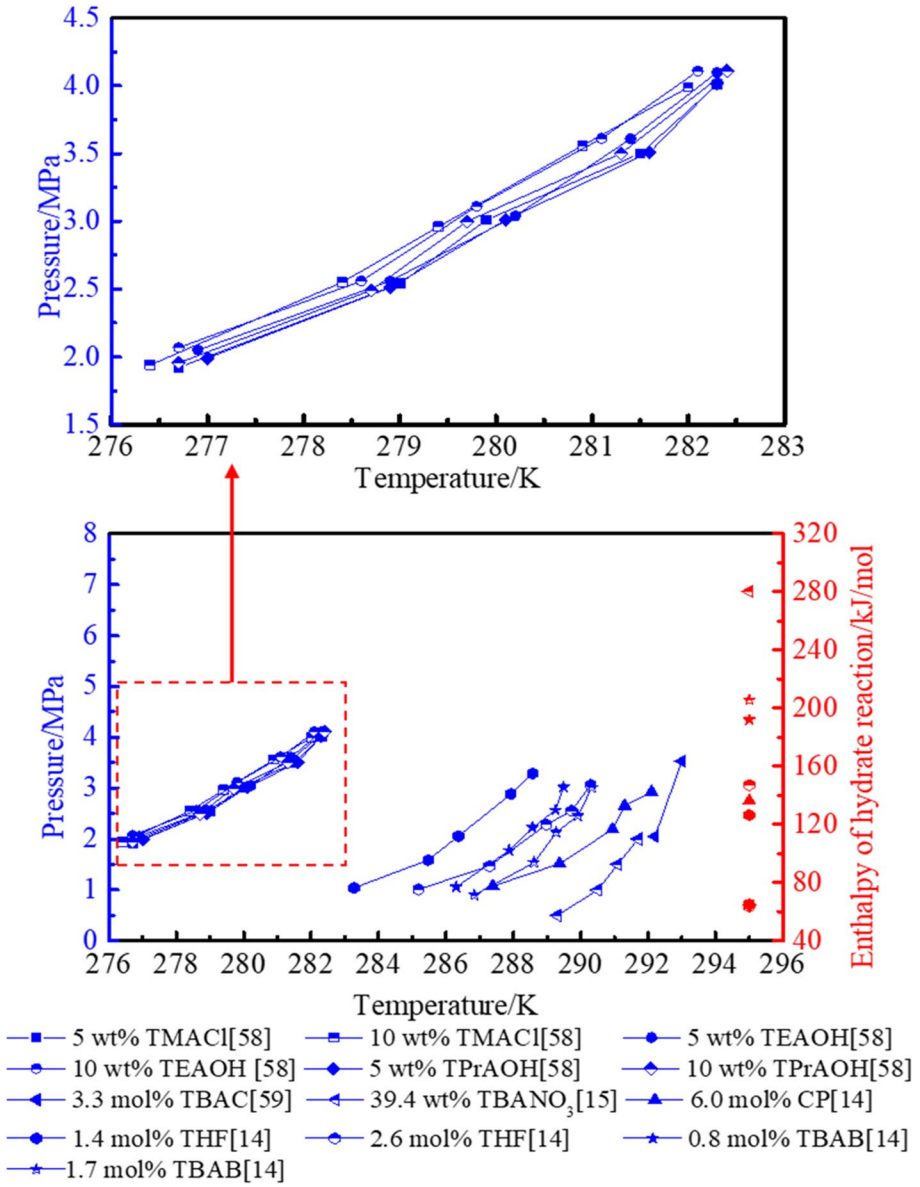

Fig. 4 Phase equilibrium pressure and temperature of CO_2 hydrates and corresponding enthalpy changes of hydrate reaction in the aqueous solution with different additives

hydrates, sI hydrates release less heat during their formation process. To prevent the generation of excess heat, kinetic promoters can be used as an alternative to thermodynamic promoters to form sI hydrates.

3 Kinetics of CO_2 hydrate formation

3.1 Kinetics of CO_2 hydrate formation in pure water and sea water

CO_2 hydrate formation is a dynamic process: initially, CO_2 dissolves into water, where it and water construct the hydrate nucleus of critical size, which subsequently develops into hydrate cages that continue to grow. For sI hydrates, CO_2 hydrate formation requires the temperature or pressure driving force. The gas storage capacity of CO_2 hydrates and the hydrate growth rate are commonly used kinetic parameters to assess the kinetics of hydrate formation, as presented in Table 1. All experiments were performed in a high-pressure stainless-steel reactor. The CO_2 hydrate formation is influenced by pressure, temperature, and salt ions in seawater. As the temperature decreases or the pressure increased, the gas storage capacity of CO_2 hydrates gradually increases, which

Table 1 A summary of hydrate formation conditions and kinetic parameters including gas storage capacity of CO_2 hydrates and hydrate growth rate in pure water and aqueous solution of NaCl

System	Equipment	NaCl concentration	T/K	P/MPa	Driving force/K	Gas storage capacity of CO_2 hydrate/(V/V)	Hydrate growth rate/(mmol CO_2/(mol H_2O·min))	Ref
Water	90 cm^3 stainless steel reactor	0 wt%	273.2	3.55	8.3	11.2	0.130	[63]
			275.2	3.55	6.3	9.9	0.120	
			277.2	3.55	4.3	8.2	0.110	
			273.2	3.05	7.2	9.0	0.110	
			275.2	3.05	5.2	8.0	0.096	
			277.2	3.05	3.2	6.4	0.077	
		1 wt%	273.2	3.55	7.8	9.2	0.110	
			275.2	3.55	5.8	6.0	0.120	
		3 wt%	273.2	3.55	6.9	7.8	0.100	
			275.2	3.55	4.9	4.4	0.089	
		5 wt%	273.2	3.55	6.0	5.7	0.099	
			275.2	3.55	4.0	2.0	0.072	
0–0.6 mm particle-size sand	700 cm^3 stainless steel reactor	3.3 wt%	274.0	4.00	6.9	41.4	0.974	[24]
			277.0	4.00	3.9	18.8	1.798	
0.6–0.8 mm particle-size sand			274.0	4.00	6.9	66.7	29.778	
			277.0	4.00	3.9	29.9	1.176	
0.8–2.0 mm particle-size sand			274.0	4.00	6.9	51.1	9.790	
			277.0	4.00	3.9	40.3	10.452	
Water	450 cm^3 stainless steel reactor	0 mmol/L	274.7	3.45	7.8	42.0	0.140	[23]
		50 mmol/L	274.7	3.45	7.8	57.9	0.097	
		100 mmol/L	274.7	3.45	7.7	37.3	0.100	
		250 mmol/L	274.7	3.45	7.6	33.8	0.110	
		350 mmol/L	274.7	3.45	7.5	24.8	0.120	
		500 mmol/L	274.7	3.45	7.3	21.8	0.110	
Water	140 cm^3 stainless steel reactor	0 wt%	273.2	3.40	7.7	97.3	0.782	[64]
		3 wt%	273.2	3.40	6.4	86.8	0.456	
		5 wt%	273.2	3.40	5.5	77.8	0.417	
Clay		0 wt%	274.2	3.00	7.5	96.8	0.778	
		3 wt%	274.2	3.00	6.2	94.1	0.756	

is attributed to the increase of the driving force to promote CO_2 hydrate growth [63]. When the temperature driving force increased from 3.2 to 8.3 K, the gas storage capacity of CO_2 hydrates increased from 6.4 V/V to 11.2 V/V. Similarly, growth rate of CO_2 hydrates increased due to the increase of temperature or pressure driving force. When the temperature driving force increased from 3.2 to 8.3 K, the hydrate growth rate increased from 0.077 mmol CO_2/(mol H_2O•min) to 0.130 mmol CO_2/(mol H_2O•min) [63]. In the presence of sodium chloride (NaCl), salt ions inhibited hydrate nucleation and decreased the gas storage capacity of the hydrates [23, 63, 64]. As the concentration of salt ions increased from 1.0 wt% to 5.0 wt% at 273.2 K and 3.55 MPa, the gas storage capacity in the aqueous solution decreased from 9.2 V/V to 5.7 V/V [63], and the hydrate growth rate decreased from 0.110 mmol CO_2/(mol H_2O•min) to 0.099 mmol CO_2/(mol H_2O•min), which showed the inhibition ability of hydrate growth became more significant with higher salt concentration. When the concentration of NaCl was below 500 mmol/L, the hydrate growth rate followed an opposite trend to the change in gas storage capacity, and it did not decrease progressively with the increase of NaCl concentration [23]. Upon the addition of 5 wt% NaCl, the gas storage capacity of the hydrates decreased from 97.3 V/V to 77.8 V/V, and the hydrate growth rate declined from 0.782 mmol CO_2/(mol H_2O•min) to 0.417 mmol CO_2/(mol H_2O•min) [64]. This pronounced inhibition at higher salt concentrations is likely due to a reduction in the temperature driving force as well as structural disruption of hydrate cages caused by ionic interactions. The presence of clay was found to mitigate the inhibitory effect of NaCl, possibly due to ion adsorption on the clay surface, which reduced the effective salt concentration

in the bulk phase [64]. Likewise, quartz sand can interact with salt ions at its surface, influencing the nucleation and growth dynamics of CO_2 hydrates. Under experimental conditions of 274.0 K and 4.00 MPa, the optimal particle size for promoting hydrate formation was identified to be in the range of 0.6–0.8 mm [24]. At this particle size, the gas storage capacity increased to 66.7 V/V, and the hydrate growth rate was significantly enhanced to 29.778 mmol CO_2/(mol H_2O•min). In conclusion, although the presence of salt ions reduces the driving force for CO_2hydrate formation, the addition of quartz sand and clay can partially alleviate the inhibitory effect of salinity on CO_2 hydrate formation.

Various kinetic models have been developed to further analyze CO_2 hydrate nucleation and growth. Based on crystal theory, the nucleation model proposed by Natarajan et al. [65] described the transition from disordered water molecules to critical crystal nuclei. According to phase field theory, the nucleation rate of CO_2 hydrate was related to the nucleation barrier of all orientations and the hydrate formation temperature, which is calculated using Eq. (6) [66].

$$J_{SS} = J_0 e^{-W^*/kT} \tag{6}$$

where J_{SS} represents the rate of steady state nucleation; J_0 represents the nucleation factor, which represents also used as the prefactor in kinetic model of classical nucleation; W^* represents the work of the nucleus formation. The degree of supercooling, as a driving force, further simplified the nucleation model, which is calculated using Eq. (7) [67].

$$J = Ae^{\Delta s_e \Delta T/kT} e^{-Bt/T\Delta T^2} \tag{7}$$

where J represents the nucleation rate, Δs_e represents the dissociation entropy of a hydrate building unit at the equilibrium temperature, k represents the Boltzmann constant, ΔT represents the supercooling temperature, T represents the temperature, A represents the kinetic parameter, and B represents the thermodynamic parameter. Considering the fractal surface with a fractal dimension to characterize the roughness of CO_2 hydrate, the nucleation behavior of CO_2 gas hydrates was elucidated. The nucleation barrier $\Delta\Psi$ for the nucleation of CO_2 hydrate is calculated using Eq. (8) [68].

$$\Delta\Psi = V_e\Delta g + V_e(P_l - P_i) + \Psi_{surf} \tag{8}$$

where V_e represents the volume of the nucleus, P represents the pressure inside the nucleus, P_l represents the liquid pressure, Ψ_{surf} represents the nucleation barrier due to the creation and destruction of interface.

The hydrate growth is influenced by hydrate reaction, heat transfer, and mass transfer processes. The agitation was used to eliminate effect of mass and heat transfer and the intrinsic kinetic reaction model was proposed as Eq. (9) [69].

$$R_y(t) = \pi k_r \mu_2 (f - f_{eq}) \tag{9}$$

where $R_y(t)$ represents the macroscopic reaction rate, k_r represents the intrinsic rate constant, μ_2 represents the second moment of the particle size distribution, f represents the fugacity of the dissolved gas, f_{eq} represents the fugacity of the three-phase equilibrium.

For the growth of the hydrate film, temperature was the primary factor influencing the growth rate of the film. Therefore, heat transfer was proposed as the rate-determining step. By coupling conductive or convective heat transfer, the overall growth rate is calculated using Eq. (10) [70].

$$v\lambda^{-1} = (L\rho_h r_c)^{-1}\Delta T \tag{10}$$

where v represents the propagation rate of CO_2 hydrate film, L represents the latent heat of the hydrate formation, λ represents the thermal conductivity of the surrounding phases, ρ_h represents the mole density of the hydrate, r_c represents the curvature of the hydrate film, ΔT represents the temperature difference.

When the growth process of CO_2 hydrates was dominated by mass transfer in a tubular reactor, the CO_2 concentration served as the driving force to calculate the hydrate growth rate, as expressed in Eq. (11) [71].

$$G = k_l \rho_{sol} A_h \left(x_b^{CO_2} - x_{\text{int}}^{CO_2} \right) \tag{11}$$

where G represents the mass growth rate of CO_2 hydrates, k_l represents the mass transfer coefficient of CO_2 gas from bulk liquid to the crystal interface, ρ_{sol} represents the density of the solution, A_h represents the internal hydrate layer area where crystals grow on, $x_b^{CO_2}$ represents the mole fraction of CO_2 in the bulk liquid phase, $x_{\text{int}}^{CO_2}$ represents the mole fraction of CO_2 in the liquid–crystal layer in equilibrium. Lee et al. [64] measured the kinetic parameters of CO_2 hydrate growth in the presence of 1–5 wt% NaCl, and CO_2 and H_2O saturation were affected by the pressure distribution, which is calculated in Eq. (12).

$$\frac{n_{CO_2}}{n_{H2O,0}} = \frac{\alpha}{5.75}[1 - \exp\left(-5.75K\left(f_{\text{exp}} - f_{eq}\right)t\right)] \tag{12}$$

where n_{CO_2} is the mole of the carbon dioxide, $n_{H_2O,0}$ is the mole of the water,α is an adjustable parameter, K is the overall reaction rote constant, f_{exp} is the fugacity of the carbon dioxide in the vapor phase at the experimental

temperature and pressure conditions, f_{eq} is the fugacity of the carbon dioxide in the hydrate-liquid water–vapor three-phase equilibrium at the temperature condition, t is the lime minute.

In the presence of salt ions, the activity of water is affected by the salt ions, which in turn influences the growth of the hydrate, as shown in Eq. (13) [72].

$$\frac{dn_{gg,H}}{dt} = KA_e \Delta\mu n_{H_2O,L} \tag{13}$$

where $n_{gg,H}$ represents the number of moles of guest gas in the hydrate phase, A_e represents the effective reaction surface area, $\Delta\mu$ represents the driving force, and K represents the temperature-dependent rate constant. The driving force for the gas hydrate kinetics is considered as a function of the chemical potentials of water in the filled hydrate and the liquid phase. The chemical potentials of water in the liquid phase ($\Delta\mu_w^L(T,P)$) is estimated by Eq. 14 [73].

$$\frac{\Delta\mu_w^L(T,P)}{RT} = \frac{\Delta\mu_w^0(T,0)}{RT_0} - \int_{T_0}^{T} \frac{\Delta h_w^L(T)}{RT^2} dT + \int_0^P \frac{\Delta V_w^L}{RT^2} dP - \ln(\alpha_w) \tag{14}$$

where T_0 represents the temperature of a reference point, $\Delta\mu_w^0(T,0)$ represents the difference in standard chemical potential of water for gas hydrate at reference temperature and absolute zero pressure, Δh_w^L represents the enthalpy difference between empty hydrate cavities and liquid water, P represents the operating pressure, ΔV_w^L represents the difference between molar volume of the water in hydrate and liquid phase, and α_w represents the absolute activity of water in aqueous phase. The activity of water in aqueous phase includes the activity of water associated with the guest gas, the activity of water associated with porous media the activity of water that accounts for the influence of the salt ions.

Table 2 presents a summary of CO_2 hydrate nucleation and growth models. Experimental and modeling results indicated that the presence of salt ions disrupted the hydrogen bond network in aqueous solutions, leading to a decrease in water activity, which impeded hydrate formation. Therefore, the addition of kinetic promoters is essential to accelerate the formation of hydrates.

3.2 Kinetics of CO_2 hydrate formation with additives

The surfactants, ionic liquids and amino acids have been used as additives to enhance kinetics of CO_2 hydrate formation. CO_2 hydrate nucleation and growth in the presence of the additives are promoted by changing the local hydrogen-bonding network or the movement of CO_2 molecules and water molecules. Some additives mainly exist in the form of ions, and others exist as molecules. These anions, cations and molecules will compete for water molecules with CO_2 guest molecules. Moreover, they also interfere with the interaction between water molecules, and the interaction between CO_2 molecules and water molecules. CO_2 hydrate nucleation mechanisms include classical nucleation theory [74, 75], unstable cluster nucleation [76, 77], interface nucleation [78, 79], local-structure nucleation [80], blob nucleation [81], and two-step nucleation [82, 83], as illustrated in Fig. 5. These nucleation mechanisms reveal that hydrate nucleation requires the formation of critical nuclei, which is stabilized through interactions between guest molecules and water molecules. In the two-step hydrate nucleation mechanism, amorphous clusters transform into critical-sized nuclei through interactions between gas and water molecules in the first step. In the second step, the

Table 2 A summary of CO_2 hydrate nucleation and growth models

Formation process	Theory	Model equation	Applicable system	Reference
Hydrate nucleation	Phase field theory	$J_{SS} = J_0 e^{-W^*/kT}$	Water	[66]
	Mass transfer effect	$J = Ae^{\Delta s_e \Delta T/kT} e^{-Bt/T\Delta T^2}$		[67]
	Interface effect	$\Delta\Psi = V_e\Delta g + V_e(P_l - P_i) + \Psi_{surf}$		[68]
Hydrate growth	Intrinsic kinetic reaction	$R_y(t) = \pi k_r \mu_2 (f - f_{eq})$	Water	[69]
	Heat transfer	$v\lambda^{-1} = (L\rho_h r_c)^{-1}\Delta T$		[70]
	Mass transfer	$G = k_l \rho_{sol} A_h \left(x_b^{CO_2} - x_{\text{int}}^{CO_2}\right)$		[71]
	Mass transfer	$\frac{n_{CO_2}}{n_{H_2O,0}} = \frac{\alpha}{5.75}[1 - \exp\left(-5.75K\left(f_{\text{exp}} - f_{eq}\right)t\right)]$	Seawater	[64]
		$\frac{dn_{gg,H}}{dt} = KA_e\Delta\mu n_{H_2O,L}$		[72]
		$\frac{\Delta\mu_w^L(T,P)}{RT} = \frac{\Delta\mu_w^0(T,0)}{RT_0} - \int_{T_0}^{T} \frac{\Delta h_w^L(T)}{RT^2} dT + \int_0^P \frac{\Delta V_w^L}{RT^2} dP - \ln(\alpha_w)$		[73]

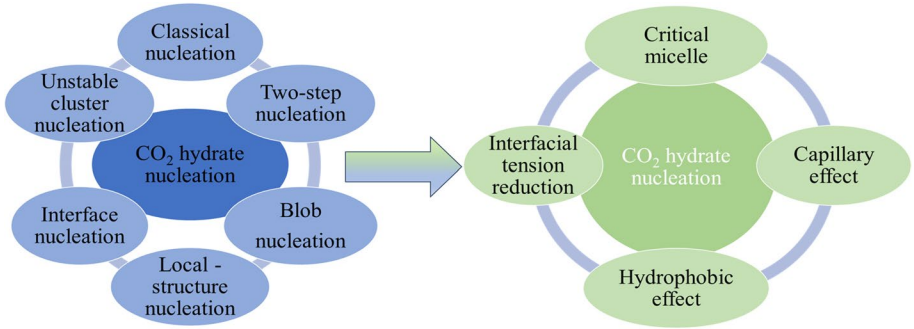

Fig. 5 CO_2 hydrate nucleation and growth theory

interconnected cavities within these nuclei absorb gas molecules to form a stable hydrate nucleus.

The hydrate growth theories include interfacial tension reduction [84–88], critical micelle formation, hydrophobic effect, and capillary effect, as illustrated in Fig. 6. Surfactants not only reduce interfacial tension between gas and liquid phases and increase gas solubility but also enhance the hydrate interface, facilitating the continuous transformation of gas and water molecules into hydrate cages [84–86]. The ice-like interfacial structure might only aid nucleation, as the hydrate shell's barrier effect prevented additional CO_2 and water molecules from accessing the hydrate surface [87]. As SDS concentration increased, more SDS anions associated with adsorbed sulfate ions through lateral interactions between hydrocarbon chains and head groups oriented toward the water phase, counteracting electrostatic repulsion among sulfate ions without significantly altering the micro-polarity

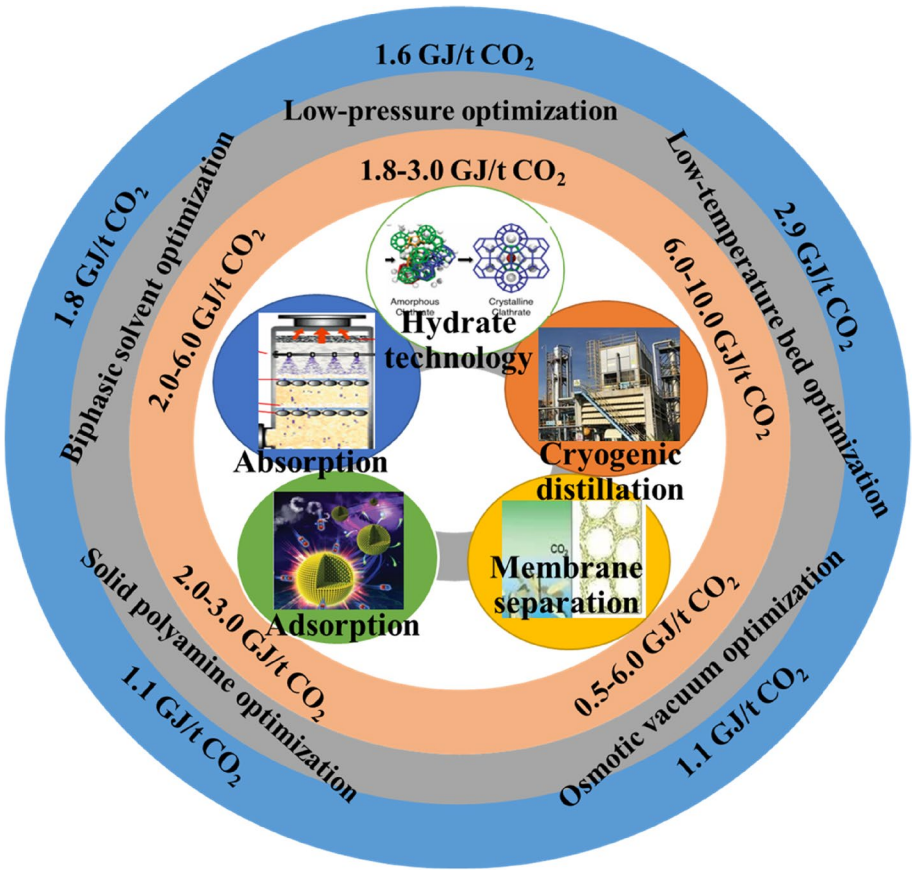

Fig. 6 Energy consumption of CO_2 capture methods from gas mixture

of the hydrate-liquid interface [89]. However, certain polymers could strengthen hydrogen bonds among surface water molecules, further restricting their transformation into clathrate hydrates and thus inhibiting hydrate growth [90–96]. The critical micelle theory has been applied to explain the role of surfactants in promoting hydrate formation. Upon reaching the critical micelle concentration (CMC) in aqueous solution, hydrate growth presented a pronounced increase [97–101]. The surfactants formed micelles with hydrophobic groups aggregating inward and hydrophilic groups arranging to create cavity structures at the CMC, which encapsulate gas molecules and increase gas solubility. Consequently, in the presence of micelles, hydrates readily formed throughout the solution. However, some researchers argued that the surfactant concentration could not reach the CMC at temperatures below the Krafft temperature, necessary for hydrate formation [102–104]. The theories of interfacial tension reduction and critical micelle concentration are based on assumptions rather than experimental evidence, complicating the explanation of hydrate formation mechanisms in the presence of additives. In fact, the hydrogen bonds among water molecules in hydrates were affected by additives, and thus the water structure played a crucial role in hydrate formation [105–116]. The water structure was enhanced near hydrophobic surfaces, exhibiting more ice-like ordering in the bulk phase or near partially hydrophobic surfaces, while it became disrupted near hydrophilic surface [109, 110]. Simulations indicated that water molecules tended to be locally structured near hydrophobic surfaces but became concave near hydrophilic surface, which could explain the preferential formation of hydrates on hydrophobic surfaces observed experimentally [111]. Dry water was used as a kinetic hydrate promoter by increasing the local contact area between water and the guest gas [117, 118]. The phenomenon of hydrate wall-climbing has been observed in aqueous solution containing surfactants and hydrophobic amino acids, so the capillary effect was applied to further elucidate the mechanism of hydrate growth and quantify the growth process [119–128]. In the absence of SDS, the lateral growth of CO_2 hydrates at the gas–liquid interface was limited, but the presence of SDS induced hydrate climbing along the reactor wall [116]. Continuous CO_2 infiltration into porous hydrate structures promoted the encapsulation efficiency of THF + CO_2 hydrate in SDS solution [123]. Nadezhda et al. [128] calculated the hydrate growth rate driven by capillary force in SDS solution, and found that the upward growth rate of CO_2 hydrate film along the reactor wall at the gas–liquid interface with low mass transfer driving force of 8×10^{-3} mm/s. In L-methionine solution, a hydrate growth model was developed based on capillary-driven mass transfer through porous hydrate structure, revealing the lateral growth rate of the CO_2 hydrate film [129]. However, the presence of NaCl inhibits the capillary effect, attributed to competition between NaCl and L-methionine for water molecules.

Liquid CO_2 exhibits higher solubility under high pressure, which plays a positive role in hydrate nucleation and growth [130, 131]. However, similar to gaseous CO_2 liquid CO_2 formed a hydrate film at the interface with liquid water, which inhibited further hydrate growth. A CO_2 hydrate film, approximately 0.4 μm thick, rapidly formed at the interface and isolated the liquid CO_2 from seawater to limit further dissolution of liquid CO_2 [132, 133]. Uchida et al. investigated the formation process of CO_2 hydrate film on the surfaces of H_2O droplets and liquid CO_2 droplets, and their results showed that this film restricted mass transfer of liquid CO_2 [134, 135]. Zhu et al. examined the effect of temperature on the initial morphology and lateral growth rate of hydrate film during the formation of liquid CO_2 hydrates, found that the rate of hydrate formation slowed with the increase of temperature [136]. At low temperatures, hydrate film growth occurred in three stages: rapid lateral growth, rapid thickening, and slow development. At higher temperatures, the growth process involved only two stages: rapid lateral growth and slow development. Moreover, the presence of salt ions significantly reduced the hydrate growth rate during the formation of CO_2 hydrates from liquid CO_2. Addressing how to enhance CO_2 hydrate storage capacity and accelerate hydrate formation rate remains a significant scientific challenge.

Table 3 provides a summary of the conditions and kinetic parameters of hydrate formation, including induction time, conversion efficiency of water to hydrate and average conversion rate of water to hydrate in the process of liquid CO_2 forming solid hydrates. Li et al. [137] found that water saturation and particle size of glass bead affected hydrate formation from liquid CO_2 by improving the contact between liquid CO_2 and liquid H_2O in the solution with 3.5 wt% NaCl at 6.0 MPa. When water saturation decreased from 60 to 40%, the conversion efficiency of water to hydrate increased from 10.0% to 20.1%, and the conversion rate of water to hydrate increased from 0.0025 mol H_2O/(mol H_2O·min) to 0.0101 mol H_2O/(mol H_2O·min). For glass beads with particle sizes below 500 μm, an increase in particle size was found to be more favorable for hydrate formation. At a constant water saturation, glass bead in the 350–500 μm size range enhanced the conversion rate of water to hydrate to 0.0116 mol H_2O/(mol H_2O·min). In contrast, when the particle size of glass bead was 1500–2500 um and water saturation was 33%, the conversion efficiency of water to hydrate and average conversion rate of water to hydrate

Table 3 A summary of hydrate formation conditions and kinetic parameters including induction time, conversion efficiency of water to hydrate and average conversion rate of water to hydrate in the process of liquid CO_2 to form solid hydrates

System	Water saturation/%	T /K	*P* /MPa	Induction time/min	Conversion efficiency of water to hydrate %	Average Conversion rate of water to hydrate/(mol H_2O/(mol H_2O·min))	Ref.
Water+3.5 wt% NaCl + 105-125 um glass bead	60	277.2	6.0	--	10.0	0.0025	[137]
Water+3.5 wt% NaCl + 105-125 um glass bead	40	277.2	6.0	--	20.1	0.0101	
Water+3.5 wt% NaCl + 177-250 um glass bead		277.2	6.0	--	20.9	0.0105	
Water+3.5 wt% NaCl + 350-500 um glass bead		277.2	6.0	--	23.2	0.0116	
Water + 288ppm SDS + 1500-2500 um glass bead	33	274.0	6.0	6.4	1.4	0.00055	[138]
Seawater + 150-250 μm glass bead	100	274.2	4.0	10.0	59.3	0.0033	[140]
Seawater + 0.15 wt% SiO_2+ 150-250 μm glass bead		274.2	4.0	5.0	80.3	0.0067	
Seawater + 0.05 wt% SDS+ 150-250 μm glass bead		274.2	4.0	34.0	70.6	0.0059	
Seawater + 0.05 wt% SDS0.15 wt% SiO_2+ 150-250 μm glass bead		274.2	4.0	18.0	64.9	0.0054	
Water	100	274.2	6.4	120.0	58.0	0.00081	[141]
Water + stirring		274.2	6.4	30.0	82.6	0.0013	
Water+300 ppm L-tryptophan		274.2	6.4	15.0	93.4	0.0023	
Water+500 ppm L-tryptophan		274.2	6.4	15.0	98.8	0.0035	
Water+1000 ppm L-tryptophan		274.2	6.4	15.0	98.6	0.0043	
Water	100	288.7	6.0	35.4	17.9	0.00022	[100]
Water+0.5 wt% SL		288.0	6.0	23.1	24.3	0.00030	
Water+1.0 wt% SL		288.0	6.0	21.1	31.8	0.00039	
Water+3.0 wt% SL		288.0	6.0	25.2	28.5	0.00035	
Brine	100	274.6	10.0	19.8	25.0	0.00017	[142]
Brine + 500 ppm L-tryptophan		274.6	10.0	33.0	19.2	0.00016	
Silica sand + water	100	274.2	4.0	10.0	91.8	0.0077	[143]
Silica sand + 300 ppm L-tryptophan		274.2	4.0	5.0	93.8	0.0078	

decreased to 1.4% and 0.00055 mol H_2O/(mol H_2O·min) respectively [138]. Almenningen et al. [139] developed a direct imaging method for pores in a micromodel chip, and revealed that CO_2 hydrate growth could occur at the phase interface or within dissolved water following the injection of liquid CO_2 into unsaturated water sandstone. The conversion rate of water to hydrate increased to 0.0059 mol H_2O/(mol H_2O·min) in the system of seawater and 150–250 μm glass bead by combining SiO_2 nanoparticles with SDS due to the heterogeneous interfaces of nanoparticles to decrease the energy barrier for hydrate nucleation and accelerate mass transfer [140].

To avoid polluting marine environment, environmental-friendly additives were developed to shorten induction time of hydrate nucleation and promote hydrate growth. The induction time of hydrate nucleation was shortened within 30.0 min in the presence of sodium lignosulfonate (SL) and L-tryptophan [100, 141]. SL was used to increase the conversion efficiency of water to hydrate from 17.9% to 31.8%, and increase the average conversion rate of water to hydrate from 0.00022 mol H_2O/(mol H_2O·min) to 0.00039 mol H_2O/(mol H_2O·min) due to the presence of micelle with SL [100]. L-tryptophan with hydrophilic carboxyl groups was introduced to achieve the conversion efficiency of water to hydrate of 98.6% and the average conversion rate of water to hydrate of 0.0043 mol H_2O/(mol H_2O·min) at the pressure of 6.4 MPa and the temperature of 274.2 K [141]. However, the presence of salt ions in the aqueous solution significantly disabled L-tryptophan and decreased average conversion rate of water to hydrate to 0.00016 mol H_2O/(mol H_2O·min) at 10.0 MPa [142]. Under optimal conditions with porous media, the induction time was shortened to 5.0 min and average conversion rate of water to hydrate was increased to 0.0078 mol H_2O/(mol H_2O·min) [143]. The formation of a hydrate cap layer has

also been investigated to assess marine sealing capacity. In unsealed marine sediment, the maximum CO_2 storage density in mud systems reached 66.8 kg/m^3, which was 60% and 67% higher than in sandy and clay systems, respectively [144]. The construction of a CO_2 hydrate cap layer further enhanced CO_2 sequestration capacity by trapping liquid CO_2 beneath the cap layer [145–148]. When the initial water saturation exceeded 26.2%, CO_2 hydrates formed within minutes, effectively halting leakage [145]. The saturation of granular hydrates formed in seawater-saturated zones was 25% lower than that of sheet-like hydrates formed in seawater residual zones [149]. Moreover, the presence of marine organic matter favored the liquid CO_2 to form hydrate [150]. Numerical simulation models indicated that increasing reservoir pore volume and reducing hydrate-induced blockage significantly increased storage capacity [151, 152]. Simulations suggested that higher flow rate and pressure accelerated hydrate formation, thereby reducing the risk of injection well blockage and enhancing the stability of the hydrate cap [153]. Whether CO_2 hydrates can effectively prevent liquid CO_2 leakage largely depends on the absolute permeability of the selected marine region [154].

4 Energy consumption and cost of CO_2 capture and sequestration

4.1 Energy consumption of CO_2 capture and sequestration

Beyond the foundational research on CO_2 capture and storage (CCS), energy consumption and cost analysis are essential for evaluating its industrial feasibility. For binary gas mixtures, the theoretical minimum work for separation can be calculated as shown in Eq. 17 [155]. The gas mixture and its components were assumed to behave as ideal gases, and the separation process was conducted under isothermal conditions. At 298 K, the minimum work required to separate 1 ton of CO_2 from a CO_2 and N_2 mixture with CO_2 mole fraction of 12% to 25% ranges from 0.12 and 0.16 GJ. The minimum work required to separate 1 ton of CO_2 from a CO_2 and methane (CH_4) mixture with a CO_2 mole fraction of 25% to 60% ranges from 0.06 to 0.12 GJ. The minimum work required to separate 1 kg of CO_2 from a CO_2 and hydrogen (H_2) mixture with a CO_2 mole fraction of 30% to 50% is 0.07 to 0.11 GJ. CO_2 and CH_4 gas mixture and CO_2 and H_2 gas mixture with higher CO_2 concentrations require less work for separation compared to CO_2 and nitrogen (N_2) gas mixture, indicating that they are easier to separate. However, in practical processes, energy consumption for CO_2 capture is also affected by gas properties and process conditions.

$$W_{\min,T} = -RT\left[\frac{x\ln x + (1-x)\ln(1-x)}{x} - \frac{y\ln y + (1-y)\ln(1-y)}{y}\right] \quad (15)$$

In the Eq. 15, R is the thermodynamic constant, valued at 8.314 J/(mol·K); T represents the thermodynamic temperature in the separation process, K; x and y are the mole fractions of a component in a binary gas mixture before and after separation, respectively.

Some researchers have systematically analyzed various CO_2 capture methods, including absorption, adsorption, cryogenic distillation, membrane separation, and hydrate technology, as shown in Fig. 6. During the chemical absorption of CO_2 using ammonia solution for gas treatment of 1000 tonnes/day, the regeneration process was energy-intensive, with an energy consumption of 2.0–6.0 GJ per ton of CO_2 absorbed [156]. Shen et al. [157] use a biphasic solvent, triethylenetetramine (TETA)-N,N,N',N'-tetramethyl-1,3-propanediamine (TMPDA), to enhance CO_2 absorption with a gas flow rate of 200 mL/min in 500 mL double-stirred cell reactor. The energy consumption associated with the absorption process was estimated by evaluating three components: reaction heat, sensible heat, and latent heat, while excluding the energy contributions from gas compression and solvent pumping. The energy consumption with the biphasic solvent was reduced to 1.8 GJ per ton of CO_2, which was 52% lower than that of the conventional monoethanolamine (MEA) absorbent. Similarly, in the adsorption process using solid materials, such as molecular sieves, porous carbon materials, metal–organic frameworks (MOFs), and covalent organic frameworks (COFs), substantial energy was required for adsorbent regeneration, consuming 2.0–3.0 GJ per ton of CO_2 separated [158]. The energy consumption was calculated based on thermal energy losses. The flue gas source was a 500 MW coal-fired power plant, with an annual CO_2 emission of approximately 3.636 Mt. A three-bed adsorption column system was employed to simulate the CO_2 capture process. Each adsorption bed was packed to a height of 1 m with an inner diameter of 7.7 cm. The pilot-scale experimental setup was designed to approximate realistic operating conditions and assess the performance of the adsorption system. In a three-column fixed bed and rotary bed system, the use of solid polyamines reduced the regeneration temperature to 348 K, decreasing the energy cost for adsorbent regeneration to 1.1 GJ per ton of CO_2 [159]. In membrane separation, energy was required for compressors and vacuum pump, with an energy demand of 0.5–6.0 GJ per ton of CO_2 separated [160]. Compared to compression configurations, a permeate vacuum configuration decreased operational energy consumption from 1.67 GJ per ton of CO_2 to 1.06 GJ per ton of CO_2 [161]. In the energy consumption analysis of this membrane separation, the efficiencies of the compressor, expander, and vacuum pump were assumed to be 85%.

In the process of CO_2 separation via cryogenic distillation, low-temperature condensation transformed gaseous CO_2 into a liquid phase, requiring continuous compression and cooling to drive phase change in the gas mixture, resulting in an energy consumption of 6.0–10.0 GJ per ton of CO_2 separated [162]. A dynamically operated low-temperature packed bed biogas treatment process with biogas flow of 0.312 kg/s further achieved energy demand of 2.9 GJ per ton of CO_2 [163]. The energy consumption was estimated based on the calculated energy requirements for compression, cooling, and air recovery, without accounting for additional energy losses. For hydrate-based CO_2 separation, compression and low-temperature cooling are also energy-intensive, consuming 1.8–3.0 GJ per ton of CO_2 separated [164–166]. The energy consumption for a fixed-bed column under static conditions was reported to be 1.4 GJ per ton of CO_2, which was lower than that of a stirred tank reactor (2.3 GJ per ton of CO_2) and a reciprocating impact reactor (5.3 GJ per ton of CO_2). A CO_2/N_2 gas mixture, derived from post-desulfurization and denitrification treatment, was used as simulated flue gas at a flow rate of 10 kmol/h. The temperature and pressure of the gas mixture were maintained at 323.0 K and 0.1 MPa, respectively. During the separation of a 10,000 Nm^3/h gas mixture containing 64 mol% CH_4 and 36 mol% CO_2, by reducing the hydrate formation pressure from 4.0 MPa to 1.0 MPa, total energy consumption was decreased by 22.3%, with energy costs reduced to 1.6 GJ per ton of CO_2 [155]. Although the analysis excluded the potential and kinetic energy of the process streams, the second law of thermodynamics was applied to evaluate energy transformation, transfer, utilization, and loss, thereby providing insights into strategies for improving both process efficiency and energy utilization.

To further calculate the costs of CO_2 capture, Baxter et al. [167] applied the concept of Levelized Cost of Electricity (LCOE) to comprehensively compare the costs of various capture methods including fuel costs, fixed and variable operation and maintenance costs, capital charge costs, and storage and monitoring costs. Figure 7 shows the cost of CO_2 capture methods from gas mixtures including cooling, steam, chemicals, electricity and capital charge costs. The flue gas was derived from a 600 MW coal-fired power plant, with a treatment capacity of 635 kg/s. For the chemical absorption process, the capital cost included major components such as blowers, compressors, heat exchangers, circulation pumps, reboilers, and dryers. The cost of packing materials was estimated based on a steel price of 1200$ per ton. Installation costs were calculated by applying a manual labor factor to the total equipment cost. Operating costs encompassed electricity consumption by blowers, compressors, heat exchangers, circulation pumps, and reboilers, as well as the cost of chemical additives. Depreciation, interest, labor, and maintenance were collectively estimated as 20% of the total annual capital investment. For membrane separation, the capital cost consisted of membranes, compressors, and expanders. In the case of cryogenic distillation, the equipment cost included blowers, compressors, heat exchangers, and distillation columns. For hydrate-based separation, the capital cost was primarily composed of

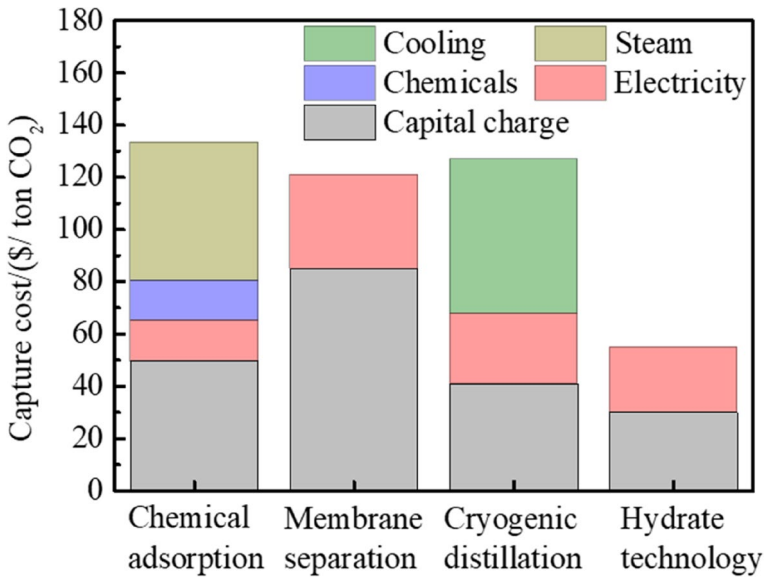

Fig. 7 Cost of CO_2 capture methods from gas mixtures including cooling, steam, chemicals, electricity and capital charge costs

compressors, heat exchangers, and hydrate reactors. In the case of amine absorption, the costs of capital charge and steam energy consumption represented significant cost components, resulting in an overall capture cost of 133.4 $ per ton of CO_2, which was higher than that of membrane separation, cryogenic distillation, and hydrate technology [168], as shown in Fig. 7. Membrane separation incurred relatively high fixed capital charge costs due to the high price of membranes. In contrast, the capture cost of hydrate technology was reduced to 55.0 $ per ton of CO_2 [169]. Capital costs were also influenced by operating conditions. At a flow rate of 100 m^3/h, the capital costs for pressure swing adsorption, water washing, and chemical absorption were 11.9 k$/($m^3/h$), 11.5 k$/(m^3/h), and 10.9 k$/($m^3/h$), respectively [170]. At a higher flow rate of 1400 m^3/h, the capital cost for cryogenic distillation was 2.6 k$/($m^3/h$), slightly above that of standard membrane technology at 2.2 k$/($m^3/h$) [171]. In terms of energy consumption and capture cost, hydrate technology demonstrates a clear advantage over other capture methods.

4.2 Cost of CO_2 capture and sequestration

The overall energy consumption and costs of total oceanic CO_2 sequestration are composed of four main components: CO_2 capture, storage, transportation, and injection into seafloor. After the selection of a suitable CO_2 capture method, various storage options are available, including high-pressure liquid CO_2 storage (HPLCD), optimized liquid CO_2 storage (OLCD), and hydrate-based CO_2 storage (HCD). Table 4 presents a summary of the cost analysis for CO_2 storage, transportation, and injection after capture. For feed gas flow rate of 3751 kmol/h, the specific energy consumption for HPLCD, OLCD, and HCD was 95.8, 89.5, and 61.4 kWh per ton of CO_2, respectively, with the total annual cost estimated at 7.7, 7.2, 5.0 $ per ton of CO_2, respectively [172]. In the optimization of the three CO_2 storage scenarios, the processes were assumed to operate under thermodynamic equilibrium and steady-state conditions. The gas phase was modeled as an ideal gas, and potential gas leakage was considered negligible. This suggested that hydrate-based storage was a promising approach for CO_2 sequestration. For CO_2 transportation of 3 Mt CO_2/year, the cost of transporting 1 million tons of CO_2 per year was estimated at 33.0 $ and 28.0 $ per ton at an approximate distance of 530 km by pipeline and 724 km by ship, respectively [173]. The cost of pipeline transport was estimated based on the compression in the capture plant, onshore and offshore pipelines, and booster. The required pressure in the well head was assumed to be 100 bar, and the onshore pipelines were also assumed to be buried 1 m underground. The cost of ship transport included the liquefaction process in the capture plant, carrier, and pumping process for injection. The ship speed was assumed to be 15 knots, and the loading and unloading times were assumed to be 20 h each. The cost of terminal included the storage tank and pressurization process of ship-transported CO_2 for offshore pipeline transport. The total energy demand for CO_2 capture, transportation, and sequestration was 16.6 MW, with hydrate-based gas separation accounting for 70% of the total energy requirement in the hydrate CO_2 capture and sequestration process [174]. When the CO_2 handling capacity reached 1 Mt CO_2/year and the transport distance exceeded 1000 km, transport costs by pipeline ranged from 0.02 to 0.04 $ per ton of CO_2 per km, by ship from 0.03 to 0.08 $ per ton of CO_2 per km, and by tank at approximately 0.1 $ per ton of CO_2 per km [175, 176].

For the injection of liquid CO_2, shallow environment for platform and jack-up rigs, medium-depth environment for semi-submersible rig and drillship, and deep-sea environment for casing while drilling (CWD), dual gradient drilling (DGD), managed pressure drilling (MPD), and managed pressure casing drilling (MPCD) are suitable [178]. Considering that drilling and initial capital investment represent the primary cost components of offshore CO_2 injection, the overall sequestration cost can be reasonably estimated based on drilling expenditures. At a depth of 3000 m and 500 m offshore, the costs of CO_2 injection using mobile ships and floating platforms were estimated at 15.2 and 12.8 $ per ton of CO_2, respectively [177]. According to the U.S. Department of Energy, sequestration costs for reservoir injection projects ranged from 8 to 20.0 $ per ton of CO_2 [179]. For a marine CO_2 sequestration project with an annual storage capacity of 1 million tons, the total cost was estimated at 36.0 $ per ton CO_2, with an initial capital investment of 150.0 million $ and a

Table 4 Cost analysis of CO_2 storage, transportation and injection after CO_2 capture

CO_2 storage methods [167]	Cost ($/ton)	CO_2 transportation methods [175, 176]	Cost ($/ton/km)	CO_2 injection methods [177]	Cost ($/ton)
HPLCD	7.7	Pipeline	0.02–0.04	Moving ship	15.2
OLCD	7.2	Ship	0.03–0.08	Floating platform	12.8
HCD	4.9	Tanker	0.1	–	–

daily energy requirement of 713 MWh [180]. The capital expenditure considered in this study included fixed capital investment, working capital, and startup costs.

The fixed capital investment and working capital covered the installation costs of key equipment such as gas compressors, bubble column reactors, refrigeration systems, and water pumps, as well as expenses related to land acquisition, water intake and discharge infrastructure, site development, auxiliary facilities, insurance, freight, taxes, engineering services, project development, and risk contingency fees. Working capital also accounted for one month's supply of raw materials, accounts receivable, accounts payable, and tax obligations. Startup costs included expenditures for commissioning labor and revenue losses incurred during process ramp-up and initial system debugging.

Globally, numerous CO_2 capture and sequestration pilot projects have been initiated, with estimated cost ranging between 50 $ and 100 $ per ton of CO_2 [181]. The cost of oceanic CO_2 sequestration ranged from 4.7 $ to 12.0 $ per ton of CO_2, roughly double that of terrestrial sequestration [182]. For self-sealing oceanic sequestration, the cost was approximately three times higher than for land-based sequestration, with cost increasing further when cumulative capacities exceeded 500 Mt/y [183]. In this sequestration scenario, the net-to-gross ratio of the target region was assumed to be approximately 2.0%, with a permeability of 22 mD. The average cost of self-sealing oceanic sequestration was 142 $ per ton of CO_2, which was significantly higher than the 57.9 $ per ton of CO_2 for non-self-sealing oceanic sequestration. With the increase of ocean depth, factors such as net sand thickness in marine sediments, construction of water injection wells, and pipeline infrastructure lead to substantial increase in oceanic sequestration cost. Marine drilling costs were influenced by drilling depth, distance from shore, and water depth [184]. While the cost of land-based sequestration was less than 100,000 $ per day, the cost for oceanic sequestration increased to between 600,000 $ and 800,000 $ per day [185]. Reducing the depth of oceanic sequestration from around 1000 m to approximately 400 m can reduce sequestration cost by nearly half, decreasing the average cost to 28.9 $ per ton of CO_2. Decreasing CO_2 capture cost, reducing transport distances, increasing storage capacity, and decreasing CO_2 injection costs can significantly reduce the cost of oceanic CO_2 sequestration [186].

5 Perspectives

Fundamental research and economic analysis reveal that hydrate-based CO_2 capture and sequestration are feasible and economical, but there are still a series of challenges: (1) The lack of comprehensive discussion on the thermodynamics and kinetics of CO_2 hydrate formation; (2) The controversy surrounding CO_2 hydrate nucleation and growth theories; (3) The limitation of hydrate-based CO_2 capture and sequestration development due to cost.

The presence of salt ions significantly alters the thermodynamics of CO_2 hydrate formation, not only shifting the hydrate phase equilibrium line but also reducing the enthalpy change of the hydrate formation reaction. Upon the addition of additives, the transformation of the hydrate structure also has a significant impact on both the phase equilibrium and the enthalpy change of hydrate formation reaction. However, there is a lack of thermodynamic studies on hydrate formation in complex systems where both seawater and additives coexist, and no unified thermodynamic model has been developed for further evaluation.

The kinetics of CO_2 hydrate formation is influenced by salt ions due to the change in water activity, thereby impacting the hydrate nucleation and growth. CO_2 hydrate nucleation and growth theories differ based on the additives. A unified theory to comprehensively explain the formation process of CO_2 hydrates is still lacking, as studies primarily rely on isolated experimental observations and results. Furthermore, there is an ongoing debate between the interfacial tension reduction theory and the critical micelle theory. Therefore, more molecular simulations and characterization experiments are essential to elucidate the CO_2 hydrate formation mechanism.

The overall energy consumption and cost of oceanic CO_2 sequestration comprise four main components with CO_2 capture, storage, transportation, and injection into seafloor. However, most studies have focused on optimizing the cost of individual component without considering the cost optimization of the entire sequestration chain. The cost of marine CO_2 injection is notably higher than that of terrestrial sequestration. The formation of hydrate caps is conducive to cost-effective CO_2 sequestration in shallow seas, which can significantly reduce the energy consumption and capital charge cost requirements for sequestration. From an economic perspective, hydrate-based oceanic carbon sequestration presents considerable sequestration potential.

Nomenclature

CO_2	Carbon dioxide
$CO_2(g)$	Gas CO_2
$nH_2O(s)$	Solid ice
$CO_2 \bullet nH_2O(s)$	Solid hydrate
$CO_2(l)$	Liquid CO_2
$nH_2O(l)$	Liquid water
P	Phase equilibrium pressure
T	Phase equilibrium temperature

ΔH_{dis}	Hydrate dissociation enthalpy
ΔV	Volume change for reaction
n	Moles of water
$x(CO_2)$	Molar fraction of CO_2 dissolves in the water
$V(CO_2)$	Volume of CO_2
CP	Cyclopentane
CP-one	Cyclopentanone
CP-ol	Cyclopentanol
DXN	1,4-dioxane
THF	Tetrahydrofuran
MCP	Methylcyclopentane
DMB	3,3-dimethyl-1-butanol
NH	Neopentane
TBAB	Tetrabutylammonium bromide
TBAC	Tetrabutylammonium chloride
TBAF	Tetrabutylammonium fluoride
TBA^+	Tetrabutylammonium ions
TMACl	Tetramethylammonium chloride
TEAOH	Tetraethylammonium hydroxide
TPrAOH	Tetrapropylammonium hydroxide
NaCl	Sodium chloride
J_{SS}	Rate of steady state nucleation
J_0	Nucleation factor
W^*	Work of the nucleus formation
J	Nucleation rate
Δs_e	Dissociation entropy of a hydrate building unit at the equilibrium temperature
k	Boltzmann constant
ΔT	Supercooling temperature
A	Kinetic parameter
B	Thermodynamic parameter
ΔΨ	Nucleation barrier
V_e	Volume of the nucleus
P_l	Liquid pressure
Ψ_{surf}	Nucleation barrier
$R_y(t)$	Macroscopic reaction rate
k_r	Intrinsic rate constant
μ_2	Second moment of the particle size distribution
f	Fugacity of the dissolved gas
f_{eq}	Fugacity of the three-phase equilibrium
v	Propagation rate of CO_2 hydrate film
L	Latent heat of the hydrate formation
λ	Thermal conductivity of the surrounding phases
ρ_h	Mole density of the hydrateMole density of the hydrate
r_c	Curvature of the hydrate film
G	Mass growth rate of CO_2 hydrate
k_l	Mass transfer coefficient of CO_2 gas
ρ_{sol}	Density of the solution
A_h	Internal hydrate layer area
$x_b^{CO_2}$	Mole fraction of CO_2 in the bulk liquid phase
$x_{\text{int}}^{CO_2}$	Mole fraction of CO_2 in the liquid-crystal layer in equilibrium
n_{CO_2}	Mole of the carbon dioxide
$n_{H_2O,0}$	Mole of the water
α	Adjustable parameter
K	Overall reaction rote constant
f_{exp}	Fugacity of the carbon dioxide in the vapor phase
f_{eq}	Fugacity of the carbon dioxide in the hydrate-liquid water-vapor three-phase equilibrium
$n_{gg,H}$	Number of moles of guest gas in the hydrate phase
A_e	Effective reaction surface area
Δμ	Driving force
$\Delta\mu_w^L(T,P)$	Chemical potentials of water in the liquid phase
$\Delta\mu_w^0(T,0)$	Difference in standard chemical potential of water for gas hydrate
Δh_w^L	Enthalpy difference between empty hydrate cavities and liquid water
ΔV_w^L	Difference between molar volume of the water in hydrate and liquid phase
a_w	Absolute activity of water in aqueous phase
CMC	Critical micelle concentration
SL	Sodium lignosulfonate
$W_{min,T}$	Energy consumption
x	Mole fractions of a component in a binary gas mixture before separation
y	Mole fractions of a component in a binary gas mixture after separation
CH_4	Methane
H_2	Hydrogen
N_2	Nitrogen
TETA	Triethylenetetramine
TMPDA	N,N,N′,N′-tetramethyl-1,3-propanediamine
MEA	Monoethanolamine
COFs	Covalent organic frameworks
LCOE	Levelized Cost of Electricity
HPLCD	High-pressure liquid CO_2 storage
OLCD	Optimized liquid CO_2 storage
HCD	Hydrate-based CO_2 storage
CWD	Casing while drilling
DGD	Dual gradient drilling
MPD	Managed pressure drilling
MPCD	Managed pressure casing drilling

Acknowledgements
This work is supported by the Key Research and Development Program of Guangzhou (no. 202206050002). All authors are thankful to the Foundation and acknowledge their support.

Authors' contributions
F.P. Liu performed the data analysis and wrote the manuscript. Y.H. Wang, X.M. Lang and G. Li reviewed and edited the manuscript. S.S. Fan conceived this review and revised the manuscript. All authors read and approved the final manuscript.

Funding
Open access funding provided by South China University of Technology.
This work was supported by the Key Research and Development Program of Guangzhou (no. 202206050002).

Data availability
The date and materials are available upon reasonable request.

Declarations

Ethics approval and consent to participate
All authors certify that the manuscript is original and not submitted to other journals.

Consent for publication
All authors agree to the publication of this manuscript.

Competing interests
All authors declare that they have no known competing financial interests or personal relationships that could have appeared to influence the work reported in this paper.

Received: 29 December 2024 Revised: 19 May 2025 Accepted: 11 June 2025
Published online: 21 July 2025

References

1. Ekaterina G, Li J (2024) Analysis of decarbonization path in New York state and forecasting carbon emissions using different machine learning algorithms. Carbon Neutrality 3:8

2. National Oceanic and Atmospheric Administration (NOAA); 2024. https://www.esrl.noaa.gov/gmd/ccgg/trends/global.html
3. Zhao C-Y, Ju S-H, Xue Y, Tao T, Ji Y, Chen X (2022) China's energy transitions for carbon neutrality: challenges and opportunities. Carbon Neutrality 1:7
4. Zhu X-N, Xiao J, Wang C-G, Zhu L-J, Wang S-R (2022) Global warming potential analysis of bio-jet fuel based on life cycle assessment. Carbon Neutrality 1:25
5. Filonchyk M, Petersond MP, Zhang L-F, Hurynovich V, He Y (2024) Greenhouse gases emissions and global climate change: Examining the influence of CO_2, CH_4, and N_2O. Sci Total Environ 935:173359
6. Hulme M (2016) 1.5 °C and climate research after the Paris Agreement. Nat Clim Change 6:222–224
7. House K-Z, Schrag D-P, Harvey C-F, Lackner K-S (2006) Permanent carbon dioxide storage in deep-sea sediments. Applied Physical Sciences 103:12291–12295
8. Schrag D-P (2007) Preparing to Capture Carbon. Science 315:812–813
9. Qanbaria F, Pooladi-Darvish M, Tabatabaie S-H, Geramid S (2011) Storage of CO_2 as hydrate beneath the ocean floor. Energy Procedia 4:3997–4004
10. Bui M, Adjiman C-S, Bardow A, Anthony E-J, Boston A, Brown S, Fennell P-S, Fuss S, Galindo A, Hackett L-A, Hallett J-P, Herzog H-J, Jackson G, Kemper J, Krevor S, Maitland G-C, Matuszewski M, Metcalfe I-S, Petit C, Puxty G, Reimer J, Reiner D-M, Rubin E-S, Scott S-A, Shah N, Smit B, Trusler J-P-M, Webley P, Wilcoxx J, Dowell N-M (2018) Carbon capture and storage (CCS): the way forward. Energy Environ Sci 11:1062–1176
11. Yu Y-S, Zhang X-W, Liu J-W, Lee Y, Li X-S (2021) Natural gas hydrate resources and hydrate technologies: a review and analysis of the associated energy and global warming challenges. Energy Environ Sci 14:5611–5668
12. Kazunari O, Yoshihiro N, Kiyoteru T (1993) Formation of CO_2 hydrate in pure and sea waters. J Chem Eng Jpn 26:558–564
13. Fan S-S, Guo T-M (1999) Hydrate formation of CO_2-rich binary and quaternary gas mixtures in aqueous sodium chloride solutions. J Chem Eng Data 44:829–832
14. Mu L, Zhang Q-Y, Li X-L, Tan Q-Q, Cui Q-Y (2002) Measurements and modeling of the hydrate phase equilibria of CO_2 in the presence of promoters. Fluid Phase Equilibr 562:113548
15. Mayoufi N, Dalmazzone D, Fürst W, Delahaye A, Fournaison L (2010) CO_2 enclathration in hydrates of peralkyl-(ammonium/phosphonium) salts: Stability conditions and dissociation enthalpies. J Chem Eng Data 55:1271–1275
16. Wakatsuki M, Yamasaki A, Teng H, Yamada K, Yanagisawa Y (2000) A new ocean disposal scenario for anthropogenic CO_2: CO_2 hydrate formation in a submerged crystallizer and its disposal. Energy 25:85–96
17. Holder G-D, Cugini A-V, Warzinski R-P (2002) Modeling clathrate hydrate formation during carbon dioxide injection into the ocean. Environ Sci Technol 29:276–278
18. West O, Tsouris C, Mccallum S, Lee S (2003) Negatively buoyant CO_2-hydrate composite for ocean carbon sequestration. AIChE J 49:283–285
19. Lee S-Y, Liang L, Riestenberg D-E, West O-R, Tsouris C, Adams E-E (2003) CO_2 hydrate composite for ocean carbon sequestration. Environ Sci Technol 37:3701–3708
20. Tsouris C, Brewer P, Peltzer E, Walz P, Riestenberg D, Liang L, West O-R (2004) Hydrate composite particles for ocean carbon sequestration: Field verification. Environ Sci Technol 38:2470–2475
21. Riestenberg D-E, Tsouris C, Brewer P-G, Peltzer E-T, Walz P, Chow A-C, Adams E-E (2005) Field Studies on the formation of sinking CO_2 particles for ocean carbon sequestration: Effects of injector geometry on particle density and dissolution rate and model simulation of plume behavior. Environ Sci Technol 39:7287–7293
22. Brewer P-G, Friederich G, Peltzer E-T Jr, Orr F-M (1999) Direct experiments on the ocean disposal of fossil fuel. Science 284:943–945
23. Farhang F, Nguyen A-V, Hampton MA (2014) Influence of sodium halides on the kinetics of CO_2 hydrate formation. Energy Fuels 28:1220–1229
24. Rehman A-N, Bavoh C-B, Pendyala R, Kassim Z, Sabil K-M, Othman N-A, Lal B (2022) Kinetic insight on CO_2 hydrate formation and dissociation in quartz sand in presence of brine. Int J Greenh Gas Con 114:103582
25. Zheng J-J, Chong Z-R, Qureshi M-F, Linga P (2023) Carbon dioxide sequestration via gas hydrates: A potential pathway toward decarbonization. Energy Fuels 34:10529–10546
26. Zhang X-M, Yang H-J, Huang T-T, Li J-P, Li P-Y, Wu Q-B, Wang Y-M, Zhang P (2022) Research progress of molecular dynamics simulation on the formation-decomposition mechanism and stability of CO_2 hydrate in porous media: A review. Renew Sust Energy Rev 167:112820
27. Aminnaji M, Qureshi M-F, Dashti H, Hase A, Mosalanejad A, Jahanbakhsh A, Babaei M, Amiri A, Maroto-Valer M (2024) CO_2 gas hydrate for carbon capture and storage applications - Part 2. Energy 300:131580
28. Zhang M-J, Sun B-J, Liu S-J, Chen L-T, Gao Y-H, Wang Z-Y (2023) Review on cooperative effect of compound additives on CO_2 hydrate formation: Recent advances and future directions. Energy Fuels 37:5667–5688
29. Lee Y, Kim H, Lee W, Kang D-W, Lee J-W, Ahn Y-H (2023) Thermodynamic and kinetic properties of CO_2 hydrates and their applications in CO_2 capture and separation. J Environ Chem Eng 11:110933
30. Liu F-P, Li A-R, Qing S-L, Luo Z-D, Ma Y-L (2022) Formation kinetics, mechanism of CO_2 hydrate and its applications. Renew Sust Energy Rev 159:112221
31. Sinehbaghizadeh S, Saptoro A, Mohammadi A-H (2022) CO_2 hydrate properties and applications: A state of the art. Prog Energ Combust 93:101026
32. Cao X, Wang H, Yang K, Wu S, Chen Q, Bian J (2022) Hydrate-based CO_2 sequestration technology: Feasibilities, mechanisms, influencing factors, and applications. J Petrol Sci Eng 219:111121
33. Wang P-F, Li Y, Sun N-R, Han S-B, Wang X-M, Su Q-Q, Li Y-J, He J, Yu X-H, Du S-Y, Francisco J-S, Zhu J-L, Zhao Y-S (2024) Hydrate technologies for CO_2 capture and sequestration: Status and perspectives. Chem Rev 124:10363–10385
34. Dashti H, Yew L-Z, Lou X (2015) Recent advances in gas hydrate-based CO_2 capture. J Nat Gas Sci Eng 23:195–207
35. Zheng J-N, Yang M-J, Liu Y, Wang D-Y, Song Y-C (2017) Effects of cyclopentane on CO_2 hydrate formation and dissociation as a co-guest molecule for desalination. J Chem Thermodyn 104:9–15
36. Choi W, Lee Y, Mok J, Seo Y (2020) Influence of competitive inclusion of CO_2 and N_2 on sII hydrate-flue gas replacement for energy recovery and CO_2 sequestration. Environ Sci Technol 54:7562–7569
37. Zheng J, Bhatnagar K, Khurana M, Zhang P, Zhang B-Y, Linga P (2018) Semiclathrate based CO_2 capture from fuel gas mixture at ambient temperature: Effect of concentrations of tetra-n-butylammonium fluoride (TBAF) and kinetic additives. Appl Energy 217:377–389
38. Anderson GK (2003) Enthalpy of dissociation and hydration number of carbon dioxide hydrate from the Clapeyron equation. J Chem Thermodyn 35:1171–1183
39. Falenty A, Salamatin A-N, Kuhs W-F (2013) Kinetics of CO_2-hydrate formation from ice powders: Data summary and modeling extended to low temperatures. J Phys Chem C 117:8443–8457
40. Sabil K-M, Witkamp G-J, Peters C-J (2010) Estimations of enthalpies of dissociation of simple and mixed carbon dioxide hydrates from phase equilibrium data. Fluid Phase Equilib 290:109–114
41. Eder E, Kadinger M, Hiller S, Arzbacher S (2025) Hydrate-based carbon capture via pressure swing in a packed bed of ice. Sep Purif Technol 361:131206
42. Martínez M-C, Dalmazzone D, Fűrst W, Delahaye A, Fournaison L (2008) Thermodynamic properties of THF + CO_2 hydrates in relation with refrigeration applications. AIChE J 54:1088–1095
43. Delahaye A, Fournaison L (2006) Effect of THF on equilibrium pressure and dissociation enthalpy of CO_2 hydrates applied to secondary refrigeration. Ind Eng Chem Res 45:391–397
44. Lin W, Delahaye A, Fournison L (2008) Phase equilibrium and dissociation enthalpy for semi-clathrate hydrate of CO_2 + TBAB. Fluid Phase Equlib 264:220–227
45. Kang S-P, Lee H, Ryu B-J (2001) Enthalpies of dissociation of clathrate hydrates of carbon dioxide, nitrogen, (carbon dioxide nitrogen), and (carbon dioxide nitrogen tetrahydrofuran). J Chem Thermodyn 33:513–521
46. Fournaison L, Delahaye A, Chatti I, Petitet J-P (2004) CO_2 hydrates in refrigeration processes. Ind Eng Chem Res 43:6521–6526
47. Yoon J-H, Yamamoto Y, Komai T, Haneda H, Kawamura T (2003) Rigorous approach to the prediction of the heat of dissociation of gas hydrates. Ind Eng Chem Res 42:1111–1114

48. Hong S, Moon S, Lee Y, Lee S, Park Y (2019) Investigation of thermodynamic and kinetic effects of cyclopentane derivatives on CO_2 hydrates for potential application to seawater desalination. Chem Eng J 363:99–106
49. Shin H-J, Lee YJ, Im J-H, Han K-W, Lee J-W, Lee Y, Lee J-D, Jang W-Y, Yoon J-H (2009) Thermodynamic stability, spectroscopic identification and cage occupation of binary CO_2 clathrate hydrates. Chem Eng Sci 64:5125–5130
50. Zheng J-N, Yang M-J, Chen B-B, Song Y-C, Wang D-Y (2017) Research on the CO_2 gas uptake of different hydrate structures with cyclopentane or methyl-cyclopentane as co-guest molecules. Energy Procedia 105:4133–4139
51. Lee Y, Moon S, Hong S, Lee S, Park Y (2020) Observation of distinct structural transformation between sI and sH gas hydrates and their kinetic properties during CO_2 capture from $N_2 + CO_2$. Chem Eng J 389:123749
52. Moon S, Park S-O, Ahn Y-H, Kim H, Shin E, Hong S, Lee Y, Kwak S-K, Park Y (2018) Distinct hydrophobic-hydrophilic dual interactions occurring in the clathrate hydrates of 3,3-dimethyl-1-butanol with help gases. Chem Eng J 348:583–591
53. Uchida T, Ohmura R, Ikeda I-Y, Nagao J, Takeya S, Hori A (2006) Phase equilibrium measurements and crystallographic analyses on structure-H type gas hydrate formed from the CH_4-CO_2-neohexane-water system. J Phys Chem B 110:4583–4588
54. Rodriguez C-T, Le Q-D, Focsa C, Pirim C, Chazallon B (2020) Influence of crystallization parameters on guest selectivity and structures in a CO_2-based separation process using TBAB semi-clathrate hydrates. Chem Eng J 382:122867
55. Rodionova T-V, Komarov V-Y, Villevald G-V, Karpova T-D, Kuratieva N-V, Manakov A-Y (2013) Calorimetric and structural studies of tetrabutylammonium bromide ionic clathrate hydrates. J Phys Chem B 117:10677–10685
56. Kim S, Seo Y (2015) Semiclathrate-based CO_2 capture from flue gas mixtures: An experimental approach with thermodynamic and Raman spectroscopic analyses. Appl Energy 154:987–994
57. Oshima M, Kida M, Nagao J (2018) Hydration numbers and thermal properties of tetra-n-butyl ammonium bromide semiclathrate hydrates determined by ion chromatography and differential scanning calorimetry. J Chem Thermodyn 123:32–37
58. Shimada W, Shiro M, Kondo H, Takeya S, Oyama H, Ebinuma T, Narita H (2005) Tetra-n-butylammonium bromide-water. Acta Crystallogr C 61:65–66
59. Li Y, Gambelli A-M, Rossi F, Mei S (2021) Effect of promoters on CO_2 hydrate formation: thermodynamic assessment and microscale Raman spectroscopy/hydrate crystal morphology characterization analysis. Fluid Phase Equilib 550:113218
60. Henriques D-C, Wigent R (2020) Effect of adding lithium chloride on tetra-n-butyl ammonium chloride semiclathrate thermal stability at atmospheric pressure. J Chem Eng Data 65:3079–3090
61. Khan M-S, Bavoh C-B, Partoon B, Lal B, Bustam M-A, Shariff A-M (2017) Thermodynamic effect of ammonium based ionic liquids on CO_2 hydrates phase boundary. J Mol Liq 238:533–539
62. Qing S-L, Zhong D-L, Yi D-T, Lu Y-Y, Li Z (2018) Phase equilibria and dissociation enthalpies for tetra-n-butylammonium chloride semiclathrate hydrates formed with CO_2, CH_4, and $CO_2 + CH_4$. J Chem Thermodyn 117:54–59
63. Moeini H, Bonyadi M, Esmaeilzadeh F, Rasoolzadeh A (2018) Experimental study of sodium chloride aqueous solution effect on the kinetic parameters of carbon dioxide hydrate formation in the presence/absence of magnetic field. J Nat Gas Sci Eng 50:231–239
64. Lee J-W, Chun M-K, Lee K-M, Kim Y-J, Lee H (2002) Phase equilibria and kinetic behavior of CO_2 hydrate in electrolyte and porous media solutions: Application to ocean sequestration of CO_2. Korean J Chem Eng 19:673–678
65. Natarajan V, Bishnoi PR, Kalogerakis N (1994) Induction phenomena in gas hydrate nucleation. Chem Eng Sci 49:2075–2087
66. Kvamme B, Graue A, Aspenes E, Kuznetsova T, Granasy L, Toth G, Pusztai T, Tegze G (2004) Kinetics of solid hydrate formation by carbon dioxide: Phase field theory of hydrate nucleation and magnetic resonance imaging. Phys Chem Chem Phys 6:2327–2334
67. Wei Y, Nobuo M (2023) Nucleation curves of carbon dioxide hydrate in the absence of a solid wall. Energy Fuels 37:3760–3774
68. Li M-Y, Fan S-S, Wang Y-H, Lang X-M, Cheng P (2024) Heterogeneous nucleation of CO_2 hydrate: A thermodynamics analysis considering effects of wall characteristics and solution activity. Int J Heat Mass Tran 224:125285
69. Clarke M-A, Bishnoi P-R (2005) Determination of the intrinsic kinetics of CO_2 gas hydrate formation using in situ particle size analysis. Chem Eng Sci 60:695–709
70. Uchida T, Ebinuma T, Kawabata J (1999) Microscopic observations of formation processes of clathrate-hydrate films at an interface between water and carbon dioxide. J Cryst Growth 204:348–356
71. Zhou H-X, Ferreira C-I (2017) Effect of type-III Anti-Freeze Proteins (AFPs) on CO_2 hydrate formation rate. Chem Eng Sci 167:42–53
72. Palodkar A-V, Jana A-K (2019) Growth and decomposition mechanism of clathrate hydrates in the presence of porous media and seawater: Experimental validation. Energy Fuels 33:1433–1443
73. Rehman A-N, Bavoh C-B, Khan M-Y, Ansari M, Lal B (2025) Unveiling the potential of CO_2 hydrates in porous media: A review on kinetic modelling, molecular dynamics simulations, and machine learning. Fuel 381:133650
74. Englezos P, Bishnoi P-R (1988) Gibbs free energy analysis for the supersaturation limits of methane in liquid water and the hydrate-gas-liquid water phase behavior. Fluid Phase Equilibr 42:129–140
75. Kelton K-F (1991) Crystal nucleation in liquids and glasses. Solid State Phys 45:75–177
76. Muller-Bongartz B, Wildeman T-R, Sloan E-D (1992) In a hypothesis for hydrate nucleation phonemena. The Second International Offshore and Polar Engineering Conference San Francisco, California, USA
77. Christiansen R-L, Sloan E-D (1994) Mechanisms and kinetics of hydrate formation. Ann N Y Acad Sci 715:283–305
78. Kvamme B (1996) A new theory for the kinetics of hydrate formation. In proceedings of 2nd international conference on natural gas hydrates, 1996.
79. Moon C, Taylor P-C, Rodger P-M (2003) Molecular dynamics study of gas hydrate formation. J Am Chem Soc 125:4706–4707
80. Radhakrishnan R, Trout B-L (2002) A new approach for studying nucleation phenomena using molecular simulations: application to CO_2 hydrate clathrates. J Phys Chem A 117:1786–1796
81. Jacobson L-C, Hujo W, Molinero V (2010) Nucleation pathways of clathrate hydrates: Effect of guest size and solubility. J Phys Chem B 114:13796–13807
82. Vatamanu J, Kusalik P-G (2010) Observation of two-step nucleation in methane hydrates. Phys Chem Chem Phys 12:15065–15072
83. Barnes B-C, Knott B-C, Beckham G-T, Wu D-T, Sum A-K (2014) Reaction coordinate of incipient methane clathrate hydrate nucleation. J Phys Chem B 118:13236–13243
84. Gómez-Díaz D, Navaza J-M, Sanjurjo B (2009) Mass-transfer enhancement or reduction by surfactant presence at a gas-liquid interface. Ind Eng Chem Res 48:2671–2677
85. Hebrard G, Zeng J, Loubiere K (2009) Effect of surfactants on liquid side mass transfer coefficients: A new insight. Chem Eng J 148:132–138
86. Lo C, Zhang J, Somasundaran P, Lee J-W (2012) Investigations of surfactant effects on gas hydrate formation via infrared spectroscopy. J Colloid Interface Sci 376:173–176
87. Stern L-A, Kirby S-H, Durham W-B (1996) Peculiarities of methane clathrate hydrate formation and solid-state deformation, including possible superheating of water ice. Science 273:1843
88. Zhang J-S, Lo C, Somasundaran P, Lu S, Couzis A, Lee J-W (2008) Adsorption of sodium dodecyl sulfate at THF hydrate/liquid interface. J Phys Chem C 112:12381–12385
89. Zhang J-S, Lo C, Somasundaran P, Lee J-W (2010) Competitive adsorption between SDS and carbonate on tetrahydrofuran hydrates. J Colloid Interface Sci 341:286–288
90. Zeng H, Wilson L-D, Walker V-K, Ripmeester J-A (2003) The inhibition of tetrahydrofuran clathrate hydrate formation with antifreeze protein. Can J Phys 81:17–24
91. Knight C-A (2000) Adding to the antifreeze agenda. Nature 406:249–250
92. Zeng H, Moudrakovski I-L, Ripmeester J-A, Walker V-K (2007) Effect of antifreeze protein on nucleation, growth and memory of gas hydrates. AIChE J 52:3304–3309

93. Sa J-H, Kwak G-H, Lee B-R, Park D-H, Han K, Lee K-H (2013) Hydrophobic amino acids as a new class of kinetic inhibitors for gas hydrate formation. Sci Rep 3:2428
94. King H-E, Hutter J-L, Lin M-Y, Sun T (2000) Polymer conformations of gas-hydrate kinetic inhibitors: a small-angle neutron scattering study. J Chem Phys 112:2523–2532
95. Moon C, Taylor P-C, Rodger P-M (2003) Clathrate nucleation and inhibition from a molecular perspective. Can J Phys 81:451–457
96. Moon C, Hawtin R-W, Rodger P-M (2007) Nucleation and control of clathrate hydrates: Insights from simulation. Faraday Discuss 136:367–382
97. Zhong Y, Rogers R-E (2000) Surfactant effects on gas hydrate formation. Chem Eng Sci 55:4175–4187
98. Lin W, Chen G-J, Sun C-Y, Guo X-Q, Wu Z-K, Liang M-Y, Chen L-T, Yang L-Y (2004) Effect of surfactant on the formation and dissociation kinetic behavior of methane hydrate. Chem Eng Sci 59:4449–4455
99. Bhattacharjee G, Kushwaha O-S, Kumar A, Khan M-Y, Patel J-N, Kumar R (2017) Effects of micellization on growth kinetics of methane hydrate. Ind Eng Chem Res 56:3687–3698
100. Huang H-L, Liu X-J, Lu H-F, Xu C-L, Zhao J-Z, Li Y, Gu Y-H, Yin Z-Y (2024) Introducing sodium lignosulfonate as an effective promoter for CO_2 sequestration as hydrates targeting gaseous and liquid CO_2. Advances in Applied Energy 14:100175
101. Wang F, Guo G, Liu G-Q, Luo S-J, Guo R-B (2016) Effects of surfactant micelles and surfactant-coated nanospheres on methane hydrate growth pattern. Chem Eng Sci 144:108–115
102. Zhang J-S, Lee S, Lee J-W (2007) Kinetics of methane hydrate formation from SDS solution. Ind Eng Chem Res 46:6353–6359
103. Di Profio P, Arca S, Germani R, Savelli G (2005) Surfactant promoting effects on clathrate hydrate formation: Are micelles really involved? Chem Eng Sci 60:4141–4145
104. Ando N, Kuwabara Y, Mori YH (2012) Surfactant effects on hydrate formation in an unstirred gas/liquid system: An experimental study using methane and micelle-forming surfactants. Chem Eng Sci 73:79–85
105. Sloan E-D, Koh C-A (2008) Clathrate Hydrates of Natural Gases, 3rded. Crc Press-Taylor & Francis Group: Boca Raton, FL 119:1–701
106. Salsh M-R, Koh C-A, Sloan E-D, Sum A-K, Wu DT (2009) Microsecond simulations of spontaneous methane hydrate nucleation and growth. Science 326:1095–1098
107. Grdadolnik J, Merzel F, Avbelj F (2017) Origin of hydrophobicityand enhanced water hydrogen bond strength near purely hydro-phobic solutes. Proc Natl Acad Sci 114:322–327
108. Chandler D (2005) Interfaces and the driving force of hydrophobic assembly. Nature 437:640–647
109. Li H-J, Stanwix P, Aman Z, Johns M, May E, Wang L-G (2016) Raman spectroscopic studies of clathrate hydrate formation in the presence of hydrophobized particles. J Phys Chem A 120:417–424
110. Kumar A, Bhattacharjee G, Kulkarni B-D, Kumar R (2015) Role of surfactants in promoting gas hydrate formation. Ind Eng Chem Res 54:12217–12232
111. Nguyen N-N, Nguyen A-V, Steel K-M, Dang L-X, Galib M (2017) Interfacial gas enrichment at hydrophobic surfaces and the origin of promotion of gas hydrate formation by hydrophobic solid particles. J Phys Chem C 121:3830–3840
112. Arjmandi M, Chapoy A, Tohidi B (2007) Equilibrium data of hydrogen, methane, nitrogen, carbon dioxide, and natural gas in semi-clathrate hydrates of tetrabutyl ammonium bromide. J Chem Eng Data 52:2153–2158
113. Nguyen N-N, Nguyen A-V, Nguyen K-T, Rintoul L, Dang L-X (2016) Unexpected inhibition of CO_2 gas hydrate formation in dilute TBAB solutions and the critical role of interfacial water structure. Fuel 185:517–523
114. Ohidi B, Danesh A, Todd A-C, Burgass R-W, Ostergaard K-K (1997) Equilibrium data and thermodynamic modelling of cyclopentane and neopentane hydrates. Fluid Phase Equilib 138:241–250
115. Piatkowski L, Zhang Z, Backus E-H-G, Bakker H-J, Bonn M (2014) Extreme surface propensity of halide ions in water. Nat Commun 5:1
116. Ke W, Svartaas T-M, Kvaløy J-T, Kosberg B-R (2016) Inhibition-promotion: Dual effects of polyvinylpyrrolidone (PVP) on structure-ii hydrate nucleation. Energy Fuels 30:7646–7655
117. Wei Y, Maeda N (2024) Kinetic promotion of gas hydrate formations using dispersions. Chem Eng Sci 286:119673
118. Wang X-L, Zhang Y-X, Wang F, Yin Z-Y, Zhang Z-B, Ting V-P (2024) Unlocking the potential of hydrate-based carbon capture: A review of passive techniques for CO_2 hydrate formation promotion. Gas Science and Engineering 126:205323
119. Nesterov A-N, Reshetnikov A-M (2019) New combination of thermodynamic and kinetic promoters to enhance carbon dioxide hydrate formation under static conditions. Chem Eng J 378:122165
120. Song T-Y, Zhang J-H, Li W, Ma J, Hu S, Liu J-X, Li X-N, Hu W-F, Lan C-M, Tian G-H, Jin T-X, Han Y-X, Wang J-C, Gong J-J, Cheng C-X (2023) Rapid growth of the CO_2 hydrate induced by mixing trace tetrafluoroethane. ACS Omega 8:41232–41242
121. Partoon B, Malik S-N-A, Azemi M-H, Sabil K-M (2013) Experimental investigations on the potential of SDS as low-dosage promoter for carbon dioxide hydrate formation. Asia-Pac J Chem Eng 8:916–921
122. Prah B, Yun R (2018) CO_2 hydrate slurry transportation in carbon capture and storage. Appl Therm Eng 128:653–661
123. Daniel-David D, Guerton F, Dicharry C, Torre J-P, Broseta D (2015) Hydrate growth at the interface between water and pure or mixed CO_2/CH_4 gases: Influence of pressure, temperature, gas composition and water-soluble surfactants. Chem Eng Sci 132:118–127
124. Li X-S, Zhan H, Xu C-G, Zeng Z-Y, Lv Q-N, Yan K-F (2012) Effects of tetrabutyl-(ammonium/phosphonium) salts on clathrate hydrate capture of CO_2 from simulated flue gas. Energy Fuels 26:518–2527
125. Cai Y-H, Chen Y-L, Li Q-J, Li L, Huang H-X, Wang S-Y, Wang W-X (2017) CO_2 hydrate formation promoted by a natural amino acid L-methionine for possible application to CO_2 capture and storage. Energ Technol 5:1195–1199
126. Liu X-J, Ren J-J, Chen D-Y, Yin Z-Y (2022) Comparison of SDS and L-Methionine in promoting CO_2 hydrate kinetics: Implication for hydrate-based CO_2 storage. Chem Eng J 438:135504
127. Shen X-D, Shi L-L, Long Z, Zhou X-B, Liang D-Q (2016) Experimental study on the kinetic effect of N-butyl-N-methylpyrrolidinium bromide on CO_2 hydrate. J Mol Liq 223:672–677
128. Molokitina N-S, Nesterov A-N, Podenko L-S, Reshetnikov A-M (2019) Carbon dioxide hydrate formation with SDS: Further insights into mechanism of gas hydrate growth in the presence of surfactant. Fuel 235:1400–1411
129. Shen X-D, Li Y, Shen L, Zeng W-J, Zhou X-B, He J, Yin ZY, Zhang Y, Wang X-G (2024) Promotion mechanism of carbon dioxide hydrate formation by L-Methionine and its competitive effects with NaCl. Energy 302:131858
130. Sahu C, Prasad S-K, Kumar R, Sangwai J-S (2023) High-pressure rheological signatures of CO_2 hydrate slurries formed from gaseous and liquid CO_2 relevant for refrigeration, pipeline transportation, carbon capture, and geological sequestration. Sep Purif Technol 309:123087
131. Zhang X-M, Wang J-X, Yang H-J, Li J-P, Li Y-H, Wu Q-B (2022) Formation and storage characteristics of CO_2 hydrate in porous media: Effect of liquefaction amount on the formation rate, accumulation amount. Appl Therm Eng 214:118747
132. Tabe Y, Hirai S, Okazaki K (1999) Measurement of clathrate-hydrate film thickness formed at the interface between liquid CO_2 and water. Greenhouse Gas Control Technologies 4:311–315
133. Tabe Y, Hirai S, Okazaki K (2000) Measurement of CO_2 hydrate film thickness based on mass transport mechanism. J Chem Eng Jpn 33:612–616
134. Uchida T, Kawabata J (1997) Measurements of mechanical properties of the liquid CO_2-water-CO_2-hydrate system. Energy 22:357–361
135. Nakajima Y, Shirota H, Namie S (2003) Observation of CO_2 hydrate formation in high pressured water. Proceedings of the Thirteenth International Offshore and Polar Engineering Conference 1:317–320
136. Zhu Y-J, Zhang Y, Chen Y-Z, Xie Y, Zhong J-R, Wang X-H, Xiao P, Sun Y-F, Sun C-Y, Chen G-J (2024) The morphology of liquid CO_2 hydrate films at different temperatures under saturation pressure. Chem Eng J 497:154478
137. Li N, Kan J-Y, Sun C-Y, Chen G-J (2002) Hydrate formation from liquid CO_2 in a glass beads bed. Chinese J Chem Eng 43:185–191
138. Zhang L-X, Kuang Y-M, Dai S, Wang J-Q, Zhao J-F, Song Y-C (2020) Kinetic enhancement of capturing and storing greenhouse gas and volatile organic compound: Micro-mechanism and micro-structure of hydrate growth. Chem Eng J 379:122357

139. Almenningen S, Gauteplass J, Fotland P, Aastveit G-L, Barth T, Ersland G (2018) Visualization of hydrate formation during CO_2 storage in water-saturated sandstone. Int J Greenhouse Gas Control 79:272–278
140. Song Y-C, Wang S-J, Cheng Z-C, Huang M-X, Zhang Y, Zheng J-N, Jiang L-L, Liu Y (2021) Dependence of the hydrate-based CO_2 storage process on the hydrate reservoir environment in high-efficiency storage methods. Chem Eng J 415:128937
141. Qureshi M-F, Dhamu V, Usadi A, Barckholtz T-A, Mhadeshwar A-B, Linga P (2022) CO_2 hydrate formation kinetics and morphology observations using high-pressure liquid CO_2 applicable to sequestration. Energy Fuels 36:10627–10641
142. Dhamu V, Qureshi M-F, Barckholtz T-A, Mhadeshwar A-B, Linga P (2023) Evaluating liquid CO_2 hydrate formation kinetics, morphology, and stability in oceanic sediments on a lab scale using top injection. Chem Eng J 478:147200
143. Dhamu V, Qureshi M-F, Abubakar S, Usadi A, Barckholtz T-A, Mhadeshwar A-B, Linga P (2023) Investigating high-pressure liquid CO_2 hydrate formation, dissociation kinetics, and morphology in brine and freshwater static systems. Energy Fuels 37:8406–8420
144. Chen H-N, Sun Y-F, Pang W-X, Wang M-L, Wang M, Zhong J-R, Ren L-L, Cao B-J, Rao D, Sun C-Y, Chen G-J (2024) Quantitative evaluation of hydrate-based CO_2 storage in unsealed marine sediments: Viewpoint from the driving force of hydrate formation and CO_2-water contact ability. Fuel 376:132682
145. Zhao G-J, Yang M-J, Pang W-X, Gong G-J, Zheng J-N, Zhang P, Chen B-B (2022) Effects of hydrate cap on leakage prevention and capacity improvement of sub-seabed CO_2 sequestration. Chem Eng J 450:138493
146. Guo Y, Li S-X, Sun H, Wu D, Liu L, Zhang N-T, Qin X-W, Lu C (2024) Enhancing gas production and CO_2 sequestration from marine hydrate reservoirs through optimized CO_2 hydrate cap. Energy 303:131821
147. Pang W-X, Chen M-Q, Fu Q, Ge Y, Zhang X-H, Wen H-Y, Zhou S-W, Li Q-P (2024) A comparative study of hydrate-based CO_2 sequestration at different scales. Energy Fuels 38:16599–16609
148. Chen J-Z, Mei S-H (2023) Gas-saturated carbon dioxide hydrates above sub-seabed carbon sequestration site and the formation of self-sealing cap. Gas Sci Eng 111:204913
149. Liu Y-Y, Xu H-Z, Sun L-T, Ma X-N, Li H-W, Jiang L-L, Zheng J-N, Song Y-C (2024) CO_2 hydrate formation characteristics inside seawater residual/saturated sediments under marine CO_2 storage scenes. Energy 309:132991
150. Liu F-P, Wang Y-H, Lang X-M, Li G, Fan S-S (2024) Hydrate formation and dissociation of liquid CO_2 with seawater containing organic matters in sand. Energy Fuels 38:17750–17760
151. Liu Z, Xu J-C, Li H-Y, Li S-X, Fan X-W (2023) Numerical investigation of CO_2 storage capacity via hydrate in deep-sea sediments. Energy Fuels 37:18996–19010
152. Yamaguchi A-J, Sato T, Tobase T, Wei X-R, Huang L, Zhang J, Bian J, Liu T-Y (2023) Multiscale numerical simulation of CO_2 hydrate storage using machine learning. Fuel 334:126678
153. Sun H-R, Chen J, Ji X, Karunakaran G, Chen B, Ranjith P-G, Song Y-C, Yang M-J (2024) Optimizing CO_2 hydrate storage: Dynamics and stability of hydrate caps in submarine sediments. Appl Energy 376:124309
154. Sawano Y, Wako T, Sato T, Tada K (2022) Numerical simulation of the effect of gas hydrate formation on liquid-CO_2 leakage suppression in sub-seabed sand sediment. Int J Greenh Gas Control 119:103728
155. Huang H, Fan S-S, Wang Y-H, Lang X-M, Li G (2023) Energy and exergy efficiency analysis for biogas De-CO_2 with tetra-n-butylammonium bromide hydrates. Energy 265:126365
156. Favre E (2007) Carbon dioxide recovery from post-combustion processes: Can gas permeation membranes compete with absorption? J Membr Sci 294:50–59
157. Shen Y, Jiang C, Zhang S, Chen J, Wang L, Chen J (2018) Biphasic solvent for CO_2 capture: Amine property-performance and heat duty relationship. Appl Energy 230:726–733
158. Zhang J, Webley P-A, Xiao P (2008) Effect of process parameters on power requirements of vacuum swing adsorption technology for CO_2 capture from flue gas. Energy Convers Manage 49:346–356
159. Gao J-B, Yan J, Song X-Y, Gao Y-K, Deng G-F, Wang Z-C, Cao L-D (2023) Utilizing solid polyamines in a rotary bed to capture CO_2 in an energy and cost-efficient manner. React Chem Eng 8:2086–2096
160. Mondal M-K, Balsora H-K, Varshney P (2012) Progress and trends in CO_2 capture/separation technologies: A review. Energy 46:431–441
161. Li Q-H, Wu H-Y, Wang Z, Wang J-X (2002) Analysis and optimal design of membrane processes for flue gas CO_2 capture. Sep Purif Technol 298:121584
162. Copenhagen Accord (2009) Decision 2/CP.15: Copenhagen Accord. Geneva: UNFCCC
163. Tuinier M-J, Annaland M (2012) Biogas purification using cryogenic packed-bed technology. Ind Eng Chem Res 51:5552–5558
164. Fang S-Q, Zhang X-Y, Zhang J-Y (2020) Evaluation on the natural gas hydrate formation process. Chinense J Chem Eng 28:881–888
165. Tajima H, Yamasaki A, Kiyono F (2004) Energy consumption estimation for greenhouse gas separation processes by clathrate hydrate formation. Energy 29:1713–1729
166. Zang X-Y, Li H, He Y, Zhou X-B, Wu N-Y, Fan S-S, Chen Y, Liang D-Q (2024) Energy efficiency analysis of hydrate and ionic liquid-based binary gas separation processes. Energy Fuels 38:22278–22289
167. Baxter L, Baxter A, Burt S (2009) Cryogenic CO_2 capture as a cost-effective CO_2 capture process. International Pittsburgh Coal Conference.
168. Tuinier M-J, Hamers H-P, Annaland M (2011) Techno-economic evaluation of cryogenic CO_2 capture-A comparison with absorption and membrane technology. Int J Greenh Gas Control 5:1559–1565
169. Rezaei N, Mohebbi V, Feyzi V (2022) Hybrid hydrate processes for CO_2/H_2 mixture purification: A techno-economic analysis. Int J Hydrogen Energ 47:10137–10155
170. Bioenergy I (1999) Biogas upgrading and utilization Task 24:6475–6481
171. Hagen M, Polman E, Myken A, Jensen J, Joensson O, Dahl A (2001) Adding gas from biomass to the gas grid. Final report.
172. Xu Z-X, Lang X-M, Fan S-S, Li G, Wang Y-H (2024) Design and optimization of carbon dioxide storage technology: Energy efficiency and economic analysis. Energy Fuels 38:7108–7120
173. Kang K, Seo Y, Chang D, Kang S, Huh C (2015) Estimation of CO_2 Transport costs in south korea using a techno-economic model. Energies 8:2176–2196
174. Prah B, Anokye M, Yun R (2023) Energy consumption analysis of hydrate based technology in the carbon capture storage process. J Mech Sci Technol 37:6727–6737
175. Luo J, Xie Y, Hou MZ, Xiong Y, Wu X, Luddeke C-T, Huang L (2023) Advances in subsea carbon dioxide utilization and storage. Energy Rev 2:100016
176. Stolaroff J-K, Pang S-H, Li W, Kirkendall W-G, Goldstein H-M, Aines R-D, Baker S-E (2021) Transport cost for carbon removal projects with biomass and CO_2 storage. Front Energy Res 9:639943
177. Caldeira K, Akai M, Brewer P, Chen B, Haugan P, IWama T, Johnston P, Kheshgi H, Li Q, Ohsumi T, Pörtner H, Sabine C, Shirayama Y, Thomson J, Barry J, Hansen L, Young B-D, Joos F. IPCC special report on carbon dioxide capture and storage (ocean storage). 2018. https://www.ipcc.ch/site/assets/uploads/2018/03/srccs_chapter6–1.pdf
178. Sahu C, Kumar R, Sangwai J-S (2020) Comprehensive review on exploration and drilling techniques for natural gas hydrate reservoirs. Energy Fuels 34:11813–11839
179. James R-I (2019) Cost and performance baseline for fossil energy plants volume 1: bituminous coal and natural gas to electricity, Pittsburgh, PA 60
180. Bhati A, Hamalian M, Bahadur V (2025) Techno-economic modeling of carbon dioxide hydrate formation for carbon sequestration. Appl Energy 377:124491
181. Kintisch E (2016) Underground injections turn carbon dioxide to stone. Science
182. Hendriks C, Graus W, van Bergen F (2004) Global carbon dioxide storage potential and costs. Report No. EEP-02001. Ecofys, Utrecht
183. Eccles J-K, Pratson L (2013) Economic evaluation of offshore storage potential in the US exclusive economic zone. Greenh Gases Sci Technol 3:84–95
184. Kumar Y, Sangwai J-S (2023) Environmentally sustainable large-scale CO_2 sequestration through hydrates in offshore basins: ab initio comprehensive analysis of subsea parameters and economic perspective. Energy Fuels 37:8739–8764

185. Amado L (2013) Reservoir Exploration and Appraisal; Energy and power in Physical sciences and engineering of Elsevier, ISBN: 9781856178549
186. Shen M-H, Kong F-L, Lige Tong L-G, Luo Y, Yin S-W, Liu C-P, Zhang P-K, Wang L, Chu P-K, Ding Y-L (2022) Carbon capture and storage (CCS): Development path based on carbon neutrality and economic policy. Carbon Neutrality 1:37

Publisher's Note